

***Ab initio* prediction of vacancy properties in concentrated alloys: The case of fcc Cu-Ni**

Xi Zhang and Marcel H. F. Sluiter\*

*Department of Materials Science and Engineering, Delft University of Technology, Mekelweg 2, 2628 CD Delft, The Netherlands*

(Received 12 August 2014; revised manuscript received 30 April 2015; published 20 May 2015)

Vacancy properties in concentrated alloys continue to be of great interest because nowadays *ab initio* supercell simulations reach a scale where even defect properties in disordered alloys appear to be within reach. We show that vacancy properties cannot generally be extracted from supercell total energies in a consistent manner without a statistical model. Essential features of such a model are knowledge of the chemical potential and imposition of invariants. In the present work, we derive the simplest model that satisfies these requirements and we compare it with models in the literature. As illustration we compute *ab initio* vacancy properties of fcc Cu-Ni alloys as a function of composition and temperature. *Ab initio* density functional calculations were performed for SQS supercells at various compositions with and without vacancies. Various methods of extracting alloy vacancy properties were examined. A ternary cluster expansion yielded effective cluster interactions (ECIs) for the Cu-Ni-Vac system. Composition and temperature dependent alloy vacancy concentrations were obtained using statistical thermodynamic models with the *ab initio* ECIs. An Arrhenius analysis showed that the heat of vacancy formation was well represented by a linear function of temperature. The positive slope of the temperature dependence implies a negative configurational entropy contribution to the vacancy formation free energy in the alloy. These findings can be understood by considering local coordination effects.

DOI: [10.1103/PhysRevB.91.174107](https://doi.org/10.1103/PhysRevB.91.174107)

PACS number(s): 61.72.Bb, 61.66.Dk, 82.60.Lf, 61.72.jd

**I. INTRODUCTION**

Nowadays, *ab initio* prediction of point defects and diffusivities in pure metals have become commonplace. Especially for self-diffusion and for impurity diffusion in dilute alloys, generally good agreement has been found with experimental data [1–8]. For point defects in pure metals, generally excellent agreement with high temperature experimental data can be achieved provided that sufficient thermal excitation effects are included [9–11]. Point defects in alloys are more complicated than point defects in pure metals due to the multiple local environments. In so far alloys have been considered, it is usually in the low-point defect concentration limit so that point defects can be assumed to be noninteracting. Within these limitations, point defect properties in ordered structures such as B2-AlNi [12–16], B2-FeAl [12,17,18], and L1<sub>2</sub>-Ni<sub>3</sub>Al [19] have been theoretically studied. As described in Refs. [14,19], special attention should be paid to the definition of the single defect formation energy for ordered alloys because it is nontrivial to define and compute supercell energy differences under the constraints of a constant number of atoms and constant degree of order. Therefore, the common strategy to solve this problem is to minimize a grand canonical potential (i.e., fixed number of lattice sites and varying number of atomic species). In this approach chemical potentials are used as Lagrange multipliers to preserve composition. Oftentimes in energy considerations little thought is given then to the requirement of preservation of, e.g., volume, as atoms in the reservoir are exchanged with the supercell. Likewise other parameters are oftentimes not clearly defined with respect to what state variables are held fixed (pressure or volume; entropy or temperature, order parameter, or ordering energy). Nevertheless, this method has found widespread use when dealing with ordered structures.

In disordered crystalline materials, such as substitutional alloys, experimental information on vacancies and diffusivities is scarce (see, e.g., Refs. [20,21]), and from the theoretical side also, there have been rather few studies that deal with specific alloy systems. Initially using empirical potentials [22–25], and later through *ab initio* approaches, both through supercell calculations [26–29] and *ab initio* based cluster expansions [30–33], it has been established that the local atomic environment around a vacancy plays a significant role. While the influence of vacancies on phase stability [30,34] and kinetics [31–33] received some attention for Al-Ni [30], Sc-S [34], and Al-Li [31–33] alloys, the actual vacancy properties in specific alloys were mostly neglected with the exception of an empirical potential study of Cu-Ni alloys by Zhao *et al.* [24]. In the latter study [24] vacancies were studied with an embedded atom method (EAM) potential and structural relaxation, vibrational, and configurational effects were included. This very comprehensive approach did not lead to a clear identification of how the structural, configurational, and vibrational effects individually contributed to vacancy properties, and the complexity of the treatment did not allow one to extract rules of thumb that might be extrapolated to other alloy systems. On the other hand, there are various lattice gas models that treat vacancies through Bragg-Williams or quasicheical approaches [14,35–41] that are transparent enough to extract rules of thumb. But these studies suffer from a too simple representation of the energetics, such as including pairwise nearest neighbor interactions only, that are applicable to very few actual alloys. Vacancy properties in disordered alloys were investigated also by studying vacancies embedded in an effective medium, such as that defined by the coherent potential approximation (CPA). CPA implementations such as the locally self-consistent Green's function (LSGF) method [42] or exact muffin-tin orbital (EMTO) method [43] were shown to give composition dependent vacancy properties in alloys at  $T = 0$  K. However, the CPA based methods consider the local vacancy environment only in an averaged way, and tend to

\*M.H.F.Sluiter@tudelft.nl

neglect the temperature dependence of the local environment and oftentimes neglect local structural relaxations or limit relaxation to the nearest neighbor shell.

Therefore, in the current work we will consider structural relaxation and configurational effects realistically, and attempt to describe the alloy-vacancy system in a simple enough model so that vacancy properties emerge as a function of a small number of intuitive parameters. As the vacancy concentration in disordered alloys is generally very low, we neglect intravacancy interactions and do not concern ourselves with vacancy clusters. In the following, we introduce a formalism to extract vacancy properties from supercell and cluster expansion approaches. We show how a simple cluster expansion can give rise to nontrivial vacancy properties in the alloy, such as negative configurational vacancy formation entropies and vacancy induced short range order. Finally, we give some general tendencies for vacancies in alloys based on phase separation and ordering tendencies in substitutional alloys.

## II. THEORY

We consider the problem of vacancy formation energies in disordered alloys, a problem that recently is receiving increased attention [27,28,31,33]. We limit ourselves initially to configurationally random alloys, i.e., the reference state is the configurationally random state without vacancies. This is not only for simplicity, but also because it uniformly applies to all substitutional alloys far enough above the transition temperature. The extension to alloys with short range order is briefly discussed later. To describe a defect formation energy, it is good to make a brief sojourn to the basic definition via the first law of thermodynamics:

$$\begin{aligned} dE &= \sum Y dX \\ &= TdS - PdV + \sum_i \mu_i dN_i + \epsilon_{\text{SRO}} d\eta_{\text{SRO}} \\ &\quad + \Delta E_d dN_d + \dots, \end{aligned} \quad (1)$$

where  $Y$  represents intensive variables that are system size independent, while  $X$  represents extensive variables that are proportional to system size. A matching pair of  $Y$  and  $X$  are usually referred to as conjugates. Subscript  $i$  refers to an atomic species,  $\epsilon_{\text{SRO}}$  is an effective interaction energy associated with short range order (SRO).  $\eta_{\text{SRO}}$  is an extensive short range order parameter, which could simply be a combination of the number of like atom pairs and of unlike atom pairs, while  $\Delta E_d$  is the energy and  $N_d$  is the number of a particular kind of defect. It then follows that the defect energy may be defined as

$$\Delta E_d = \left. \frac{dE}{dN_d} \right|_{S,V,N_i,\eta_{\text{SRO}}}, \quad (2)$$

where the interest lies in the parameters that are held constant, the ‘‘invariants.’’ As we generally are more apt to work at constant pressure this equation can be conveniently rewritten in terms of the enthalpy. At finite temperatures Eq. (2) needs a modification because the configurational entropy is nonanalytic in the low (defect) concentration limit. Then, the configurational entropy contribution due to the defect species

under consideration must be explicitly excluded. In the case of substitutional point defects this gives

$$\Delta \tilde{G}_d = \left. \frac{d\tilde{G}}{dN_d} \right|_{T,P,N_i,\eta_{\text{SRO}}}, \quad (3)$$

where the excess Gibbs energy is defined in the usual way, namely by excluding the ideal mixing contribution

$$\tilde{G} = G - Nk_B T [x_d \ln(x_d) + (1 - x_d) \ln(1 - x_d)], \quad (4)$$

with  $N$  representing the total number of atomic positions, and  $x_d = N_d/N$  being the fraction of atomic positions that is occupied by the point defects.

### A. Problematic supercell calculations

In order to facilitate the link with *ab initio* supercell calculations, we consider how the defect formation enthalpy  $\Delta H_d$  might be extracted from periodic supercell calculations by replacing a derivative with a finite difference. Moreover, the  $T = 0$  K case will be considered here which is typical for *ab initio* calculations. It should be emphasized that the result of this exercise is that vacancy properties in disordered, or less than perfectly ordered, alloys cannot be derived from supercell calculations alone. An additional statistical thermodynamic model is essential. At  $T = 0$  K the entropy contribution vanishes so that  $H$  takes the same value as the free energies  $G$  and  $\tilde{G}$ :

$$\Delta H_d = \left. \frac{dH}{dN_d} \right|_{T=0,P,N_i,\eta_{\text{SRO}}} = [H_{\text{sc}+d} - H_{\text{sc}}]_{T=0,P,N_i,\eta_{\text{SRO}}}. \quad (5)$$

Below, the invariants will be omitted for brevity. When the defect is a vacancy, the requirement of keeping the number of atoms constant means that an appropriate term for compensating the energy loss of the vacated atom must be included:

$$\Delta H_{\text{vac}} = [H_{\text{sc}+\text{vac}} - H_{\text{sc}} + \mu], \quad (6)$$

where  $\mu$  is the chemical potential of the vacated atom. For a pure metal  $\mu$  is simply the energy of the supercell divided by the number of atoms in the supercell. However, in a disordered alloy, say with atomic species A and B, the  $\mu$  term depends on the type of atom removed to make the vacancy. Moreover,  $\mu_i$  is the chemical potential of atomic species  $i$  ( $i = A$  or B) in the alloy, which generally differs from  $\mu_i$  in the pure element, as was erroneously assumed in Eq. (5) in Ref. [27]. It is now apparent also why an enthalpy formulation is preferable over an energy formulation because maintaining equal pressure is much easier than maintaining equal volume in the supercell with vacancy plus that of the  $i$  atom vis-a-vis the supercell without the vacancy.

In binary A-B random alloys, vacancies can be surrounded by various numbers of A and B atoms unlike the pure element case. In the nearest neighbor shell of an fcc alloy the 12 nearest neighbors of a vacancy can range from 12 A and 0 B atoms all the way to 0 A and 12 B atoms. The composition of the nearest neighbor shell, and of more distant neighbor shells, affects the vacancy formation enthalpy. It is then apparent that ‘‘the vacancy formation enthalpy’’ in a disordered alloy

requires a careful definition because the vacancy formation enthalpy must be a function of the atomic neighborhood of the vacancy, the composition of the alloy, and other factors. In order to preserve the composition of the alloy, A and B atoms need to be removed according to their composition, that is  $x_A$  times an A atom and  $x_B$  times a B atom. It follows that a weighted average over A and B removed supercells must be considered,

$$\begin{aligned} \Delta H_{\text{vac}}(x_A, x_B) &= x_A [H_{\text{sc}+\text{vac}_A} + \mu_A - H_{\text{sc}}] \\ &\quad + x_B [H_{\text{sc}+\text{vac}_B} + \mu_B - H_{\text{sc}}] \\ &= x_A [H_{\text{sc}+\text{vac}_A} - H_{\text{sc}}] \\ &\quad + x_B [H_{\text{sc}+\text{vac}_B} - H_{\text{sc}}] + H_{\text{sc}}/N \\ &= \left[ x_A H_{\text{sc}+\text{vac}_A} + x_B H_{\text{sc}+\text{vac}_B} - \frac{N-1}{N} H_{\text{sc}} \right], \end{aligned} \quad (7)$$

where  $N$  is the number of atoms in the supercell without vacancy. Of course actual supercells contain small numbers of atoms only, and therefore they poorly satisfy the invariants. Removing a certain atom from a supercell changes the composition and the state of order. For solid solutions without any short or long range order, the most configurationally representative supercells are constructed as special quasirandom structures (SQSs) which, for all presupposed important correlation functions in the alloy, reproduce the values for truly random structures [44]. In such a supercell one can then remove one atom at a time, and define the vacancy formation enthalpy as an appropriate average:

$$\Delta H_{\text{vac}}(x_A, x_B) = \frac{1}{N} \sum_{i=1}^N \left[ H_{\text{SQS-atom}_i} - \frac{N-1}{N} H_{\text{SQS}} \right]. \quad (8)$$

However, the above equation is actually not physically relevant because it averages over vacancy neighborhoods. In an actual alloy vacancies would occur where favorable local neighborhoods exist, so that the effective vacancy formation enthalpy should be tilted towards the lowest enthalpy neighborhoods. In a random alloy with low A concentration, it is improbable to find neighborhoods with exclusively A atoms, even if that type of neighborhood were to give the lowest vacancy formation enthalpy. Therefore, the tilting towards the lowest enthalpy configurations is limited by combinatorial factors. If the effective interactions between vacancies and A or B atoms are limited to the near neighbors, the sum in Eq. (8) could be limited to those atomic positions which have a particular neighborhood  $\alpha$  only,

$$\Delta H_{\text{vac}}^\alpha(x_A, x_B) = \frac{1}{N_\alpha} \sum_{i_\alpha=1}^{N_\alpha} [H_{\text{SQS-atom}_{i_\alpha}} + \mu_i - H_{\text{SQS}}]. \quad (9)$$

Where  $N_\alpha$  refers to the number of sites in the SQS supercells with neighborhood  $\alpha$ . This definition is akin to Refs. [24,43,45,46]. The chemical potentials of the A and B atomic species in the solid solution (at  $T = 0$  K) can be obtained by fitting an interpolation formula, usually some low-order polynomial in the composition, to the solid solution enthalpy. In the earlier work [45,46] the chemical potential was obtained by averaging over various ordered structures, which

for disordered alloys is likely to be less reliable than using SQSs.

In practice, it is rather cumbersome to generate SQS supercells that contain all types of neighborhoods. Just considering the nearest neighbor shell in fcc solid solutions alone gives 144 distinct configurations [47] in a binary alloy. Therefore, it is usually more efficient to compute neighborhood dependent vacancy formation enthalpies through cluster expansions [31–33].

## B. Cluster expansion

In the cluster expansion approach the A-B alloy with vacancies is treated as a ternary with the vacancy as an additional species [30–33,48,49]. As the vacancy concentration in actual disordered alloys is usually very low, and vacancy clusters in thermally equilibrated alloys are rare, such cluster expansions typically do not require determination of vacancy-vacancy interaction terms. This significantly reduces the number of effective cluster interactions (ECIs) that are needed for a good representation of the energetics of alloys with vacancies.

Here we follow the site occupation variable definition  $\mathbf{p}$  as in Refs. [50–52], where the site occupation is represented as a vector with as many components as there are species in the alloy, here vacancy, A, and B atoms. For convenience the vacancy could be designated as a type “C” atom, an idea already expressed earlier in Refs. [30,34,48,49,53,54]. The occupation variable for every site  $i$  thus has vector components  $p^{(C)}$ ,  $p^{(B)}$ , and  $p^{(A)}$ .  $p^{(Q)}$  is the probability that a site is occupied by the species  $Q$ . For a particular site  $i$ ,  $p^{(Q)}$  takes the value zero, except when the actual occupancy at that site is “Q” in which case it equals unity.

As every site is occupied by one and only one of these three species, it follows that for every site there exists a “sumrule”:  $p^{(C)} + p^{(B)} + p^{(A)} = 1$ . Therefore, one of the components is redundant. Specifying  $p^{(C)}$  and  $p^{(B)}$  fully determines the value of  $p^{(A)}$  through  $p^{(A)} = 1 - p^{(C)} - p^{(B)}$ .

Sumrules apply not just to individual sites but to clusters also. In a cluster each site is occupied by one of the species in the alloy, giving rise to the concept of a “cluster decoration” where each site in a cluster is decorated with an atomic species. The sum of the probabilities for all the cluster decorations is unity for each cluster in the alloy. For instance, the sum of probabilities for pair decorations, here for a ternary alloy:  $p^{(AA)} + p^{(AB)} + p^{(AC)} + p^{(BA)} + p^{(BB)} + p^{(BC)} + p^{(CA)} + p^{(CB)} + p^{(CC)} = 1$ .

Using these sum rules, it can be trivially shown that redundancy can be removed by eliminating the cluster decoration probabilities involving one of the species in the alloy. In other words, all cluster decoration probabilities in a ternary A-B-C alloy can be completely determined by specifying the probabilities of decorations involving the species C and B only. Generally, in an alloy with  $N_{sp}$  species, the cluster decoration probabilities involving  $N_{sp} - 1$  species can be used as a basis set of nonredundant variables, i.e., as correlation functions, to fully describe the probabilities, i.e., the configuration [55]. In the case of a binary alloy, this means that the cluster decoration probabilities of pure B cluster decorations  $p_\gamma$  (where we have eliminated the B superscripts for brevity) fully describes the configurational order, so that the enthalpy of a binary alloy

with structure  $\sigma$  can be given as

$$H^\sigma = \sum_{\gamma} J_{\gamma} p_{\gamma}^{\sigma}, \quad (10)$$

where  $\gamma$  indicates a cluster and  $J_{\gamma}$  is an effective interaction enthalpy associated with a pure B cluster decoration, as was formally proven in Ref. [55]. Considering vacancies as a ternary species, and considering isolated vacancies only, Eq. (10) can be adapted to include vacancies in alloys,

$$H^\sigma = \sum_{\gamma} J_{\gamma} p_{\gamma} + \sum_{\gamma'} J_{\gamma'} p_{\gamma'}, \quad (11)$$

where the second term involves cluster decorations  $\gamma'$  in which one B species is substituted by a vacancy. The single site term in the second sum,  $\gamma' = C$  (vacancy), pertains to the vacancy formation enthalpy in pure A  $J_C$  and the probability of finding a vacancy  $p_C$ . Of course Eqs. (10) and (11) can be written equally well in terms of the Gibbs energy excluding the configurational entropy part in terms of temperature dependent effective interactions [56].

The enthalpy of the random binary alloy is easily obtained from the cluster expansion because all the cluster decoration probabilities are products of single site decoration probabilities, that is, atomic concentrations. On the fcc lattice, considering nearest neighbor pair and nearest neighbor equilateral triangle ECIs only, this gives

$$H_{\text{rnd}}(x_B) = J_0 + x_B J_1^{(B)} + x_B^2 n_{2,1} J_{2,1}^{(BB)} + x_B^3 n_{3,1} J_{3,1}^{(BBB)}, \quad (12)$$

where  $J_0$  is a so-called empty cluster ‘‘interaction’’ which serves to define the enthalpy of pure A and  $n_{\gamma}$  is the number of clusters of type  $\gamma$  per lattice site;  $\gamma$  indicates the number of sites in a cluster, followed by a type, e.g., (2,1) for a nearest neighbor pair, (2,2) for a second nearest neighbor pair [57]. For the fcc lattice,  $n_{2,1} = 6$  and  $n_{3,1} = 8$ . The enthalpy of mixing and the formation energy of any structure  $\sigma$  is obtained by subtracting the enthalpy from the pure end members  $H_A(H_B)$ ,

$$H_{\text{mix}}(x_B) = H_{\text{rnd}}(x_B) - x_B H_B - x_A H_A, \quad (13)$$

$$H_{\text{form},\sigma}(x_B) = H_{\sigma}(x_B) - x_B H_B - x_A H_A. \quad (14)$$

The  $T = 0$  K chemical potentials of A and of B are extracted from the random enthalpy,

$$\mu_A(x_B) = J_0 - 6x_B^2 J_{2,1}^{(BB)} - 16x_B^3 J_{3,1}^{(BBB)}, \quad (15)$$

$$\begin{aligned} \mu_B(x_B) = & J_0 + J_1^{(B)} + 6x_B(2 - x_B) J_{2,1}^{(BB)} \\ & + 8x_B^2(3 - 2x_B) J_{3,1}^{(BBB)}. \end{aligned} \quad (16)$$

If the solid solution is not random, one can generate configurations that satisfy predefined degrees of long or short range order [58], e.g., through Monte Carlo algorithms. The ECIs are obtained by inverting Eq. (10) through the so-called structure inversion method, described in detail elsewhere [57,59,60]. An expression for the formation enthalpy of a vacancy in an alloy is derived from Eq. (11) by considering which bonds are broken and which bonds are created when an A or B atom is replaced by a vacancy while imposing the requirement of keeping the number of atoms constant. To include the effect

of the neighborhood, we consider an atom surrounded by a particular neighborhood  $\alpha$  formed by first, and optionally more distant neighbor shells, embedded in the alloy. Considering the nearest neighbor shell only as a neighborhood, this gives

$$\begin{aligned} \Delta H_{\text{vac}(A)}^{(\alpha)}(x_B) = & J_1^{(C)} + n_1^{(\alpha)} J_{2,1}^{(BC)} + n_2^{(\alpha)} J_{3,1}^{(BBC)} \\ & + \mu_A(x_B) - J_0, \\ \Delta H_{\text{vac}(B)}^{(\alpha)}(x_B) = & J_1^{(C)} + n_1^{(\alpha)} J_{2,1}^{(BC)} + n_2^{(\alpha)} J_{3,1}^{(BBC)} + \mu_B(x_B) \\ & - (J_0 + J_1^{(B)} + n_1^{(\alpha)} J_{2,1}^{(BB)} + n_2^{(\alpha)} J_{3,1}^{(BBB)}), \end{aligned} \quad (17)$$

where the subscript  $\text{vac}(i)$  ( $i = A$  or  $B$ ) indicates whether the vacated central atom is A (or B),  $J_1^{(C)}$  is the enthalpy needed for forming a vacancy in pure A,  $J_{2,1}^{(PQ)}$  is the effective nearest neighbor pair interaction per PQ atom pair,  $J_{3,1}^{(PQR)}$  is the effective nearest neighbor equilateral triangle interaction per PQR atom triangle, and  $n_1^{(\alpha)}(n_2^{(\alpha)})$  is the number of B atoms (BB nearest neighbor pairs) in the nearest neighbor shell around the vacancy with neighborhood  $\alpha$ . It is trivial to include more neighbor shells, and clusters with more sites. The 144 distinct nearest neighbor shell configurations [47] in fcc solid solutions in a binary alloy in this approximation are actually energetically distinguished by the numbers  $n_1^{(\alpha)}$  and  $n_2^{(\alpha)}$  only. Therefore, just 41 distinct vacancy formation enthalpies emerge for each central vacated atom A (or B) from Eqs. (17), see Table I. Of course Eqs. (17) can be generalized to the Gibbs energy of vacancy formation by using temperature dependent ECIs that account for thermal excitation effects provided that the contribution from the ideal configurational entropy is excluded. Moreover, within the cluster expansion approach the effect of short range order can be incorporated by using the cluster expansion within a lattice gas model, which can be solved using Monte Carlo [31,32] or cluster variation methods [30,48].

### C. Vacancy concentration

As seen above in Eqs. (17), the enthalpy of a vacancy defect depends on the environment  $\alpha$ , and on which atom species  $i$  is removed, A or B. The vacancy formation enthalpy in the alloy is therefore a weighted sum over environments and over removed atom species,

$$\Delta H_{\text{vac}} = \sum_{\alpha,i} x_{\text{vac}(i)}^{(\alpha)} \Delta H_{\text{vac}(i)}^{(\alpha)}, \quad (18)$$

where  $x_{\text{vac}(i)}^{(\alpha)}$  is the concentration of each type of vacancy. It is now evident also that the removed atom species index  $i$  is really needed, because the likelihood of finding an A or a B atom in environment  $\alpha$  is not the same for the two atom species. Of course, after the atom  $i$  is removed, it is no longer possible to determine what species originally was there. The concentration of vacancy types  $x_{\text{vac}(i)}^{(\alpha)}$  is a product of concentration (or probability)  $x_i^{(\alpha)}$  of finding an  $i$  atom in an  $\alpha$  environment and of the probability of removing that  $i$  atom from that environment  $f_{\text{vac}(i)}^{(\alpha)}$ . Naturally  $f_{\text{vac}(i)}^{(\alpha)}$  should be a function of  $\Delta H_{\text{vac}(i)}^{(\alpha)}$  because if the latter is large the corresponding probability should be low. There must also be an entropy associated with  $f_{\text{vac}(i)}^{(\alpha)}$ . As the vacancy defects are



TABLE I. Types of nearest neighbor shells ( $\alpha$ ) in an fcc A-B alloy: corresponding indices  $k$  from Table XIII in Ref. [47], degeneracy ( $m^{(\alpha)}$ ), number of B atoms, and BB pair ( $n_1^{(\alpha)}$  and  $n_2^{(\alpha)}$ ) in the nearest neighbor shell.

| $\alpha$ | Index $k$ [47] | $m^{(\alpha)}$ | $n_1^{(\alpha)}$ | $n_2^{(\alpha)}$ |
|----------|----------------|----------------|------------------|------------------|
| 1        | 1              | 1              | 0                | 0                |
| 2        | 2              | 12             | 1                | 0                |
| 3        | 3-5            | 42             | 2                | 0                |
| 4        | 6              | 24             | 2                | 1                |
| 5        | 7-9            | 44             | 3                | 0                |
| 6        | 10-12          | 120            | 3                | 1                |
| 7        | 13, 14         | 48             | 3                | 2                |
| 8        | 15             | 8              | 3                | 3                |
| 9        | 16, 17         | 9              | 4                | 0                |
| 10       | 18, 19         | 96             | 4                | 1                |
| 11       | 20-28          | 240            | 4                | 2                |
| 12       | 29-31          | 96             | 4                | 3                |
| 13       | 32, 33         | 54             | 4                | 4                |
| 14       | 34-38          | 108            | 5                | 2                |
| 15       | 39-44          | 264            | 5                | 3                |
| 16       | 45-52          | 264            | 5                | 4                |
| 17       | 53-55          | 120            | 5                | 5                |
| 18       | 56, 57         | 36             | 5                | 6                |
| 19       | 58-66          | 216            | 6                | 4                |
| 20       | 67-72          | 240            | 6                | 5                |
| 21       | 73-83          | 336            | 6                | 6                |
| 22       | 84, 85         | 96             | 6                | 7                |
| 23       | 86, 87         | 36             | 6                | 8                |
| 24       | 34-38          | 108            | 7                | 6                |
| 25       | 39-44          | 264            | 7                | 7                |
| 26       | 45-52          | 264            | 7                | 8                |
| 27       | 53-55          | 120            | 7                | 9                |
| 28       | 56, 57         | 36             | 7                | 10               |
| 29       | 16, 17         | 9              | 8                | 8                |
| 30       | 18, 19         | 96             | 8                | 9                |
| 31       | 20-28          | 240            | 8                | 10               |
| 32       | 29-31          | 96             | 8                | 11               |
| 33       | 32, 33         | 54             | 8                | 12               |
| 34       | 7-9            | 44             | 9                | 12               |
| 35       | 10-12          | 120            | 9                | 13               |
| 36       | 13, 14         | 48             | 9                | 14               |
| 37       | 15             | 8              | 9                | 15               |
| 38       | 3-5            | 42             | 10               | 16               |
| 39       | 6              | 24             | 10               | 17               |
| 40       | 2              | 12             | 11               | 20               |
| 41       | 1              | 1              | 12               | 24               |

few and generally far apart, the entropy can be represented by an ideal entropy,

$$\Delta S_{\text{vac}} = - \sum_{\alpha, i} k_B x_i^{(\alpha)} \Xi(f_{\text{vac}(i)}^{(\alpha)}), \quad (19)$$

with

$$\Xi(f_{\text{vac}(i)}^{(\alpha)}) = f_{\text{vac}(i)}^{(\alpha)} \ln(f_{\text{vac}(i)}^{(\alpha)}) + (1 - f_{\text{vac}(i)}^{(\alpha)}) \ln(1 - f_{\text{vac}(i)}^{(\alpha)}). \quad (20)$$

It then follows that at finite temperature, the Gibbs energy due to the formation of vacancies can be written as

$$\Delta G_{\text{vac}} = \sum_{\alpha, i} [x_{\text{vac}(i)}^{(\alpha)} \Delta H_{\text{vac}(i)}^{(\alpha)} + k_B T x_i^{(\alpha)} \Xi(f_{\text{vac}(i)}^{(\alpha)})]. \quad (21)$$

Once  $\Delta H_{\text{vac}(i)}^{(\alpha)}$  and the short range order as given by  $x_i^{(\alpha)}$  are known, the concentration of each type of vacancy  $x_{\text{vac}(i)}^{(\alpha)}$  can be computed by minimizing Eq. (21). However, the minimization of  $\Delta G_{\text{vac}}$  with respect to  $x_{\text{vac}(i)}^{(\alpha)}$  does not generally satisfy preservation of both A and B atoms. The apparent number of vacated A atoms might differ from what is to be expected on the basis of the composition. Hence, a constraint must be imposed:

$$\frac{\sum_{\alpha} x_{\text{vac}(B)}^{(\alpha)}}{\sum_{\alpha} x_{\text{vac}(A)}^{(\alpha)}} = \frac{x_B}{x_A}. \quad (22)$$

Using a Lagrange multiplier  $\lambda$  this gives a Lagrangian

$$\Lambda = \Delta G_{\text{vac}} + \lambda \left[ x_A \sum_{\alpha} x_{\text{vac}(B)}^{(\alpha)} - x_B \sum_{\alpha} x_{\text{vac}(A)}^{(\alpha)} \right], \quad (23)$$

and the values of  $x_{\text{vac}(i)}^{(\alpha)}$  are then found by solving

$$\begin{aligned} \frac{\partial \Lambda}{\partial x_{\text{vac}(i)}^{(\alpha)}} &= \Delta H_{\text{vac}(i)}^{(\alpha)} - \lambda [\delta_{iA} x_B - \delta_{iB} x_A] \\ &+ k_B T \ln \left( \frac{f_{\text{vac}(i)}^{(\alpha)}}{1 - f_{\text{vac}(i)}^{(\alpha)}} \right) = 0, \end{aligned} \quad (24)$$

where  $\delta$  is the Kronecker delta. When vacancy concentrations are small, the denominators inside the logarithm can be neglected, yielding

$$x_{\text{vac}(i)}^{(\alpha)} = x_i^{(\alpha)} \exp(-\beta \{ \Delta H_{\text{vac}(i)}^{(\alpha)} - \lambda [\delta_{iA} x_B - \delta_{iB} x_A] \}), \quad (25)$$

where  $\beta = (k_B T)^{-1}$ . By substituting Eq. (25) into (22) an analytical solution for  $\lambda$  is obtained,

$$\lambda = \frac{1}{\beta} \ln \left( \frac{x_A \sum_{\alpha} x_B^{(\alpha)} e^{-\beta \Delta H_{\text{vac}(B)}^{(\alpha)}}}{x_B \sum_{\alpha} x_A^{(\alpha)} e^{-\beta \Delta H_{\text{vac}(A)}^{(\alpha)}}} \right). \quad (26)$$

In the random alloy case,  $x_i^{(\alpha)}$  is a simple function of the composition

$$x_i^{(\alpha)} = m^{(\alpha)} x_i x_A^{12-n_1^{(\alpha)}} x_B^{n_1^{(\alpha)}}, \quad (27)$$

where  $m^{(\alpha)}$  is the degeneracy of a particular neighborhood, see Table I. In nonrandom alloys, a Monte Carlo method can be used to impose a certain degree of short or long range order on the probabilities  $x_i^{(\alpha)}$ . Of course the sum of  $x_i^{(\alpha)}$  over all  $\alpha$  yields the concentration  $x_i$ . The total vacancy concentration is obtained from

$$x_{\text{vac}}(x_B, T) = \sum_{\alpha, i} x_{\text{vac}(i)}^{(\alpha)}. \quad (28)$$

It is evident that the total vacancy concentration does not necessarily follow a simple Arrhenius equation because each neighborhood has its own vacancy formation enthalpy, see Eq. (25). At low temperature, only those  $\alpha$  with the lowest formation enthalpies contribute, while at high temperature  $\alpha$  with higher formation enthalpies contribute also. Therefore,

when the total vacancy concentration is fit to an Arrhenius equation, it is to be expected that the effective vacancy formation energy shifts towards higher values as the temperature increases. Although  $\Delta H_{\text{vac}(A)}^{(\alpha)}$  is in this derivation temperature independent, the effective energy for vacancy formation is better represented as a temperature dependent Gibbs energy

$$\Delta G_{\text{vac}}^{\text{eff}}(x_B, T) = -k_B T \ln[x_{\text{vac}}(x_B, T)]. \quad (29)$$

The temperature dependence of  $\Delta G_{\text{vac}}^{\text{eff}}$  can be used to determine an effective vacancy formation entropy  $\Delta S_{\text{vac}}^{\text{eff}}$  and enthalpy  $\Delta H_{\text{vac}}^{\text{eff}}$ ,

$$\Delta S_{\text{vac}}^{\text{eff}}(x_B) = -[\Delta G_{\text{vac}}^{\text{eff}}(x_B, T_1) - \Delta G_{\text{vac}}^{\text{eff}}(x_B, T_2)]/[T_1 - T_2], \quad (30)$$

$$\Delta H_{\text{vac}}^{\text{eff}}(x_B) = \Delta G_{\text{vac}}^{\text{eff}}(x_B, T_1) + T_1 \Delta S_{\text{vac}}^{\text{eff}}(x_B), \quad (31)$$

where  $T_1$  and  $T_2$  indicate the temperature range of interest. Another vacancy property of interest is the average number of B neighbors around a vacancy,

$$\langle n_B \rangle = \frac{1}{x_{\text{vac}}} \sum_{\alpha, i} x_{\text{vac}(i)}^{(\alpha)} n_1^{(\alpha)}. \quad (32)$$

In the above derivation, it is assumed that the fraction of neighborhoods  $x_i^{(\alpha)}$  is not affected by the vacancy concentrations  $x_{\text{vac}(i)}^{\alpha}$ . This should be true as long as  $x_{\text{vac}(i)}^{\alpha}$  is much smaller than  $x_i^{(\alpha)}$ , i.e.,  $f_{\text{vac}(i)}^{\alpha} \ll 1$ . It breaks down when, e.g., the lowest energy neighborhood  $\alpha'$  is very rare. Say if an all A surrounded vacancy is strongly favored in an almost pure B alloy. In such a case we must expect a coupling of short or long range ordering with the occurrence of vacancies. Fortunately one can explicitly verify whether  $f_{\text{vac}(i)}^{\alpha}$  is small.

### III. METHOD

The thermodynamics of fcc Cu-Ni solid solutions was investigated by means of SQSs with 16 atoms per cell with compositions  $\text{Cu}_4\text{Ni}_{12}$ ,  $\text{Cu}_{12}\text{Ni}_4$  (both structures listed as SQS-1 in Ref. [61]), and  $\text{Cu}_8\text{Ni}_8$  (two variants listed as SQS-2 and SQS-3 in Ref. [61]). The pure Cu and Ni phases are considered also using the same type cell as for the  $\text{Cu}_4\text{Ni}_{12}$  and  $\text{Cu}_{12}\text{Ni}_4$  compositions. Generalized gradient approximation [62,63] projector augmented wave pseudopotentials as implemented in VASP [64–66], version 4.6, are used with collinear spin polarization. Integrations in reciprocal space use a  $\Gamma$ -centered Monkhorst-Pack grid with the number of  $k$  points determined through  $N_{\text{atom}} N_{k \text{ point}} \approx 10\,000$  in the first Brillouin zone. Precision was set to “accurate.” In all calculations, the electronic wave functions were expanded in terms of plane waves up to a cutoff kinetic energy of 320 eV. The Hermite-Gauss smearing method of Methfessel and Paxton of order 1 has been used, with a smearing parameter of 0.1 eV. All structures are fully relaxed. The convergence criteria for energy, force magnitude, and stress component were 0.1 meV, 10 meV/nm, and 1 kbar, respectively. Structural optimizations were reinitiated at least twice. With these convergence settings energy changes between the last ionic iterations are a few  $\mu\text{eV}/\text{atom}$  only. All *ab initio* calculations pertain to  $T = 0$  K with zero-point vibrational corrections being neglected. In the

four types of SQSs every site was once replaced by a vacancy, giving rise to  $4 \times 16 = 64$  supercells with a single vacancy. A cluster expansion using point, nearest neighbor pair, and nearest neighbor equilateral triangle clusters was fit to in total 71 structures; 2 pure elements, vacuum, 4 SQSs, and 64 single vacancy SQS derived structures. The ECIs were used in a ternary cluster variation method (CVM) [67,68] calculation in the tetrahedron approximation to determine the Cu-Ni phase diagram, and the vacancy concentration as a function of composition and temperature. In the CVM calculations the ratio of Cu to Ni atoms is held constant, but the concentration of the vacancy species is freely varied. The equilibrium vacancy concentration is determined by minimizing the Gibbs energy with respect to the vacancy concentration.

## IV. RESULTS AND DISCUSSION

Vacancy properties in concentrated Cu-Ni alloys are reported and discussed. Next, we seek to generalize our findings to other alloy types, where we consider alloys that are of ordering type, unlike Cu-Ni, and alloys in which the vacancy formation enthalpy in the end members differs even more, or significantly less than for Cu-Ni.

### A. Alloy with phase separation: The case of fcc Cu-Ni

The *ab initio* computed supercell properties are listed in Table II. In the supercells with vacancies, the letters following the structure indicate which atom has been vacated, “a” (“p”) indicates that the first (16th) atom in the structure is vacated. Enthalpy of formation of the SQS, computed as described in Ref. [61], is used as a proxy for the mixing enthalpy  $\Delta H_{\text{mix}}$ . Figure 1 illustrates that the compositional dependence of the mixing enthalpy can be approximated by a subregular solution model. The chemical potential of Cu and Ni is extracted from the mixing enthalpy as a function of the alloy composition. It should be remarked that small 16 atom supercells do not give very accurate vacancy formation energies, but the objective here is not high accuracy but insight in vacancy properties in alloys. For the pure elements a comparison with literature values is given in Table III. It is evident that the results are comparable to other PBE-GGA [62,63] calculations with small supercells. We chose the PBE implementation of the GGA because a recent study [69] suggests that the PBE-GGA xc potential performs at least as well as the newer AM05-GGA [70] xc potential in describing vacancy formation energies.

In the SQSs single vacancies were introduced by removing a single atom at a time, followed by a structural relaxation. The computed enthalpies are used in Eq. (6) to extract vacancy formation enthalpies for various vacancy neighborhoods, see Fig. 2. It is evident that the greater the number of Cu atoms in the nearest neighbor shell, the smaller the vacancy formation enthalpy. This is in keeping with the greater vacancy formation enthalpy in pure Ni in comparison with that in pure Cu.

The SQS calculations with, and without vacancies, are used also for obtaining a cluster expansion. The computed ECIs, shown in Table IV, have been extracted in terms of  $n$ -body clusters ( $n = 1, 2, 3$ ). Although a much smaller number of ECIs is used than there are structural energies to be

TABLE II. Computed enthalpies ( $H$ ) and magnetic moments ( $M$ ) for supercells as described in the text, the number of Cu atoms in the nearest neighbor shell around the vacant site, the chemical potentials, and the vacancy formation enthalpy according to Eq. (6).

| Structure | Formula                          | $H$ (eV/cell) | $M$ ( $\mu_B$ /cell) | $n_1^{(\text{Cu})}$ | $\mu_{\text{Ni}}$ (eV/atom) | $\mu_{\text{Cu}}$ (eV/atom) | $H_{\text{vac}}^\alpha$ (eV) |
|-----------|----------------------------------|---------------|----------------------|---------------------|-----------------------------|-----------------------------|------------------------------|
| SQS-1     | Ni <sub>16</sub> Cu <sub>0</sub> | -89.167       | 10.031               |                     | -5.573                      | -3.538                      |                              |
| SQS-1     | Ni <sub>15</sub> Cu <sub>0</sub> | -82.185       | 9.499                | 0                   | -5.573                      |                             | 1.409                        |
| SQS-1     | Ni <sub>0</sub> Cu <sub>16</sub> | -59.563       | 0.000                |                     | -5.585                      | -3.723                      |                              |
| SQS-1     | Ni <sub>0</sub> Cu <sub>15</sub> | -54.781       | 0.000                | 12                  |                             | -3.723                      | 1.059                        |
| SQS-1     | Ni <sub>12</sub> Cu <sub>4</sub> | -81.381       | 6.054                |                     | -5.555                      | -3.674                      |                              |
| SQS-1a    | Ni <sub>11</sub> Cu <sub>4</sub> | -74.489       | 5.529                | 3                   | -5.555                      |                             | 1.337                        |
| SQS-1b    | Ni <sub>11</sub> Cu <sub>4</sub> | -74.438       | 5.658                | 1                   | -5.555                      |                             | 1.388                        |
| SQS-1c    | Ni <sub>11</sub> Cu <sub>4</sub> | -74.388       | 5.531                | 1                   | -5.555                      |                             | 1.437                        |
| SQS-1d    | Ni <sub>11</sub> Cu <sub>4</sub> | -74.588       | 5.613                | 4                   | -5.555                      |                             | 1.237                        |
| SQS-1e    | Ni <sub>11</sub> Cu <sub>4</sub> | -74.607       | 5.688                | 6                   | -5.555                      |                             | 1.219                        |
| SQS-1f    | Ni <sub>11</sub> Cu <sub>4</sub> | -74.534       | 5.680                | 5                   | -5.555                      |                             | 1.292                        |
| SQS-1g    | Ni <sub>11</sub> Cu <sub>4</sub> | -74.430       | 5.623                | 3                   | -5.555                      |                             | 1.395                        |
| SQS-1h    | Ni <sub>11</sub> Cu <sub>4</sub> | -74.342       | 5.741                | 1                   | -5.555                      |                             | 1.483                        |
| SQS-1i    | Ni <sub>11</sub> Cu <sub>4</sub> | -74.424       | 5.635                | 2                   | -5.555                      |                             | 1.402                        |
| SQS-1j    | Ni <sub>11</sub> Cu <sub>4</sub> | -74.410       | 5.680                | 2                   | -5.555                      |                             | 1.415                        |
| SQS-1k    | Ni <sub>11</sub> Cu <sub>4</sub> | -74.392       | 5.664                | 3                   | -5.555                      |                             | 1.434                        |
| SQS-1l    | Ni <sub>11</sub> Cu <sub>4</sub> | -74.536       | 5.736                | 5                   | -5.555                      |                             | 1.289                        |
| SQS-1m    | Ni <sub>12</sub> Cu <sub>3</sub> | -76.343       | 6.588                | 2                   |                             | -3.674                      | 1.363                        |
| SQS-1n    | Ni <sub>12</sub> Cu <sub>3</sub> | -76.352       | 6.580                | 3                   |                             | -3.674                      | 1.354                        |
| SQS-1o    | Ni <sub>12</sub> Cu <sub>3</sub> | -76.359       | 6.537                | 4                   |                             | -3.674                      | 1.347                        |
| SQS-1p    | Ni <sub>12</sub> Cu <sub>3</sub> | -76.304       | 6.606                | 3                   |                             | -3.674                      | 1.402                        |
| SQS-1     | Ni <sub>4</sub> Cu <sub>12</sub> | -66.873       | 0.000                | 12                  | -5.524                      | -3.730                      |                              |
| SQS-1a    | Ni <sub>4</sub> Cu <sub>11</sub> | -61.879       | 0.000                | 9                   |                             | -3.730                      | 1.264                        |
| SQS-1b    | Ni <sub>4</sub> Cu <sub>11</sub> | -62.044       | 0.001                | 11                  |                             | -3.730                      | 1.099                        |
| SQS-1c    | Ni <sub>4</sub> Cu <sub>11</sub> | -62.032       | 0.000                | 11                  |                             | -3.730                      | 1.111                        |
| SQS-1d    | Ni <sub>4</sub> Cu <sub>11</sub> | -61.842       | 0.000                | 8                   |                             | -3.730                      | 1.301                        |
| SQS-1e    | Ni <sub>4</sub> Cu <sub>11</sub> | -61.777       | 0.054                | 6                   |                             | -3.730                      | 1.366                        |
| SQS-1f    | Ni <sub>4</sub> Cu <sub>11</sub> | -61.859       | 0.000                | 7                   |                             | -3.730                      | 1.283                        |
| SQS-1g    | Ni <sub>4</sub> Cu <sub>11</sub> | -61.959       | 0.000                | 9                   |                             | -3.730                      | 1.184                        |
| SQS-1h    | Ni <sub>4</sub> Cu <sub>11</sub> | -62.113       | 0.000                | 11                  |                             | -3.730                      | 1.030                        |
| SQS-1i    | Ni <sub>4</sub> Cu <sub>11</sub> | -61.987       | 0.000                | 10                  |                             | -3.730                      | 1.156                        |
| SQS-1j    | Ni <sub>4</sub> Cu <sub>11</sub> | -62.023       | 0.000                | 10                  |                             | -3.730                      | 1.120                        |
| SQS-1k    | Ni <sub>4</sub> Cu <sub>11</sub> | -61.968       | 0.000                | 9                   |                             | -3.730                      | 1.175                        |
| SQS-1l    | Ni <sub>4</sub> Cu <sub>11</sub> | -61.866       | 0.000                | 7                   |                             | -3.730                      | 1.277                        |
| SQS-1m    | Ni <sub>3</sub> Cu <sub>12</sub> | -60.160       | 0.000                | 10                  | -5.524                      |                             | 1.188                        |
| SQS-1n    | Ni <sub>3</sub> Cu <sub>12</sub> | -60.113       | 0.000                | 9                   | -5.524                      |                             | 1.235                        |
| SQS-1o    | Ni <sub>3</sub> Cu <sub>12</sub> | -60.043       | 0.000                | 8                   | -5.524                      |                             | 1.305                        |
| SQS-1p    | Ni <sub>3</sub> Cu <sub>12</sub> | -60.192       | 0.000                | 9                   | -5.524                      |                             | 1.157                        |
| SQS-2     | Ni <sub>8</sub> Cu <sub>8</sub>  | -73.990       | 2.243                |                     | -5.527                      | -3.726                      | 1.297                        |
| SQS-2a    | Ni <sub>8</sub> Cu <sub>7</sub>  | -68.865       | 3.081                | 3                   |                             | -3.726                      | 1.400                        |
| SQS-2b    | Ni <sub>8</sub> Cu <sub>7</sub>  | -68.864       | 3.081                | 3                   |                             | -3.726                      | 1.400                        |
| SQS-2c    | Ni <sub>8</sub> Cu <sub>7</sub>  | -68.989       | 2.801                | 7                   |                             | -3.726                      | 1.275                        |
| SQS-2d    | Ni <sub>8</sub> Cu <sub>7</sub>  | -69.013       | 2.834                | 7                   |                             | -3.726                      | 1.252                        |
| SQS-2e    | Ni <sub>8</sub> Cu <sub>7</sub>  | -68.973       | 2.764                | 7                   |                             | -3.726                      | 1.291                        |
| SQS-2f    | Ni <sub>8</sub> Cu <sub>7</sub>  | -68.989       | 2.810                | 7                   |                             | -3.726                      | 1.275                        |
| SQS-2g    | Ni <sub>8</sub> Cu <sub>7</sub>  | -68.974       | 2.760                | 7                   |                             | -3.726                      | 1.290                        |
| SQS-2h    | Ni <sub>8</sub> Cu <sub>7</sub>  | -69.013       | 2.827                | 7                   |                             | -3.726                      | 1.251                        |
| SQS-2i    | Ni <sub>7</sub> Cu <sub>8</sub>  | -67.081       | 1.886                | 5                   | -5.527                      |                             | 1.382                        |
| SQS-2j    | Ni <sub>7</sub> Cu <sub>8</sub>  | -67.116       | 2.117                | 5                   | -5.527                      |                             | 1.347                        |
| SQS-2k    | Ni <sub>7</sub> Cu <sub>8</sub>  | -67.125       | 1.990                | 5                   | -5.527                      |                             | 1.338                        |
| SQS-2l    | Ni <sub>7</sub> Cu <sub>8</sub>  | -67.081       | 1.876                | 5                   | -5.527                      |                             | 1.382                        |
| SQS-2m    | Ni <sub>7</sub> Cu <sub>8</sub>  | -67.127       | 1.980                | 5                   | -5.527                      |                             | 1.336                        |
| SQS-2n    | Ni <sub>7</sub> Cu <sub>8</sub>  | -67.117       | 2.108                | 5                   | -5.527                      |                             | 1.347                        |
| SQS-2o    | Ni <sub>7</sub> Cu <sub>8</sub>  | -67.368       | 2.124                | 9                   | -5.527                      |                             | 1.095                        |
| SQS-2p    | Ni <sub>7</sub> Cu <sub>8</sub>  | -67.368       | 2.124                | 9                   | -5.527                      |                             | 1.095                        |

TABLE II. (Continued.)

| Structure | Formula                         | $H$ (eV/cell) | $M$ ( $\mu_B$ /cell) | $n_1^{(\text{Cu})}$ | $\mu_{\text{Ni}}$ (eV/atom) | $\mu_{\text{Cu}}$ (eV/atom) | $H_{\text{vac}}^\alpha$ (eV) |
|-----------|---------------------------------|---------------|----------------------|---------------------|-----------------------------|-----------------------------|------------------------------|
| SQS-3     | Ni <sub>8</sub> Cu <sub>8</sub> | -73.995       | 2.208                |                     | -5.527                      | -3.726                      |                              |
| SQS-3a    | Ni <sub>8</sub> Cu <sub>7</sub> | -68.849       | 3.071                | 3                   |                             | -3.726                      | 1.420                        |
| SQS-3b    | Ni <sub>8</sub> Cu <sub>7</sub> | -68.848       | 3.070                | 3                   |                             | -3.726                      | 1.422                        |
| SQS-3c    | Ni <sub>8</sub> Cu <sub>7</sub> | -69.045       | 2.847                | 7                   |                             | -3.726                      | 1.225                        |
| SQS-3d    | Ni <sub>8</sub> Cu <sub>7</sub> | -69.045       | 2.838                | 7                   |                             | -3.726                      | 1.224                        |
| SQS-3e    | Ni <sub>8</sub> Cu <sub>7</sub> | -69.043       | 2.882                | 7                   |                             | -3.726                      | 1.226                        |
| SQS-3f    | Ni <sub>8</sub> Cu <sub>7</sub> | -69.044       | 2.844                | 7                   |                             | -3.726                      | 1.225                        |
| SQS-3g    | Ni <sub>8</sub> Cu <sub>7</sub> | -69.043       | 2.882                | 7                   |                             | -3.726                      | 1.226                        |
| SQS-3h    | Ni <sub>8</sub> Cu <sub>7</sub> | -69.044       | 2.841                | 7                   |                             | -3.726                      | 1.225                        |
| SQS-3i    | Ni <sub>7</sub> Cu <sub>8</sub> | -67.149       | 2.010                | 5                   | -5.527                      |                             | 1.319                        |
| SQS-3j    | Ni <sub>7</sub> Cu <sub>8</sub> | -67.149       | 1.991                | 5                   | -5.527                      |                             | 1.319                        |
| SQS-3k    | Ni <sub>7</sub> Cu <sub>8</sub> | -67.155       | 2.206                | 5                   | -5.527                      |                             | 1.314                        |
| SQS-3l    | Ni <sub>7</sub> Cu <sub>8</sub> | -67.149       | 2.010                | 5                   | -5.527                      |                             | 1.320                        |
| SQS-3m    | Ni <sub>7</sub> Cu <sub>8</sub> | -67.154       | 2.206                | 5                   | -5.527                      |                             | 1.314                        |
| SQS-3n    | Ni <sub>7</sub> Cu <sub>8</sub> | -67.149       | 1.989                | 5                   | -5.527                      |                             | 1.320                        |
| SQS-3o    | Ni <sub>7</sub> Cu <sub>8</sub> | -67.422       | 1.993                | 9                   | -5.527                      |                             | 1.047                        |
| SQS-3p    | Ni <sub>7</sub> Cu <sub>8</sub> | -67.420       | 1.978                | 9                   | -5.527                      |                             | 1.049                        |

fitted to, nevertheless a rather good fit is obtained with a predictive error [67] or cross-validation score [71] of less than 4.5 meV/atom. The good performance of the CE is apparent also when the formation energies are computed from the ECIs, listed in Table IV, using Eq. (11) and plotted versus the *ab initio* computed formation energies from Eq. (14), as shown in Fig. 3. The CE reproduces the *ab initio* data with a root mean square error of less than 4 meV/atom.

The mixing enthalpy of Cu-Ni alloys as a function of composition is computed using the ECIs with Eq. (13). Figure 4 illustrates that the mixing enthalpy as estimated through Fig. 1, as computed through the formation energy of SQS, and as obtained by a phase diagram assessment using

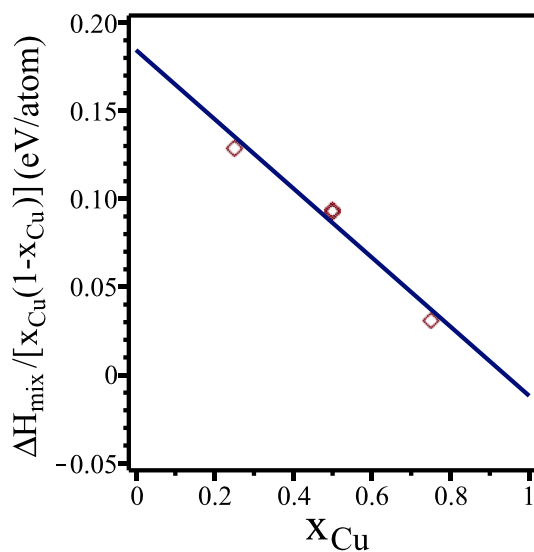


FIG. 1. (Color online)  $\Delta H_{\text{mix}}/[x_{\text{Cu}}(1-x_{\text{Cu}})]$  as a function of the atomic concentration Cu: (a) as computed with Eq. (14) using SQS formation enthalpies (diamond symbols) and (b) as interpolated through a least squares linear fit (solid line).

experimental data [72], are all in fair agreement. The tendency towards phase separation is strongest at about  $x_{\text{Cu}} = 0.4$ .

The ECIs can be used also in a cluster variation method calculation of the phase diagram, see Fig. 5. The *ab initio* computed phase diagram displays a miscibility gap with a maximum temperature of 680 K at Cu<sub>0.35</sub>Ni<sub>0.65</sub> in excellent agreement with the assessment of experimental data by an Mey in Fig. 7 of Ref. [72], which gives a maximum temperature of 640 K at Cu<sub>0.4</sub>Ni<sub>0.6</sub>, and as assessed by Chakrabarti *et al.* [73] which gives a maximum temperature of 628 K at Cu<sub>0.33</sub>Ni<sub>0.67</sub>. It should be remarked that the concentration of vacancies is so low, that even when the phase diagram was computed strictly as a binary Cu-Ni alloy without considering vacancies, the changes would have been completely imperceptible.

Local environment dependent vacancy formation enthalpies  $\Delta H_{\text{vac}(i)}^{(\alpha)}(x_{\text{Cu}})$  at  $T = 0$  K can be obtained by substituting the ECIs into Eqs. (17), see Fig. 6. It is evident that two energy

TABLE III. Vacancy formation enthalpy in fcc Cu and fcc Ni as computed with Eq. (9), and as reported in the literature.

| Method                    | $H_{\text{vac}}^{\text{Cu}}$ (eV) | $H_{\text{vac}}^{\text{Ni}}$ (eV) | Reference |
|---------------------------|-----------------------------------|-----------------------------------|-----------|
| LDA                       | 1.26                              |                                   | [69]      |
| PW91                      | 0.99                              |                                   | [69]      |
| PBE [62,63]               | 1.06                              | 1.41                              | this work |
| PBE [62,63] 16-atom cell  | 1.03                              | 1.46                              | [78]      |
| PBE [62,63] 32-atom cell  | 1.02                              | 1.46                              | [78]      |
| PBE [62,63] 32-atom cell  | 1.04                              | 1.44                              | [79]      |
| PBE [62,63] 108-atom cell | 1.06                              |                                   | [69]      |
| AM05 [70] 32-atom cell    | 1.28                              | 1.75                              | [78]      |
| AM05 [70] 32-atom cell    | 1.26                              | 1.69                              | [79]      |
| AM05 [70] 108-atom cell   | 1.29                              |                                   | [69]      |
| Experiment                | 0.92–1.27                         | 1.45–1.8                          | [20]      |
| Experiment                | 1.04–1.49                         |                                   | [80]      |
| Experiment                |                                   | 1.2–1.68                          | [81]      |
| Experiment (LGT DD+PAS)   | 1.06                              |                                   | [69]      |



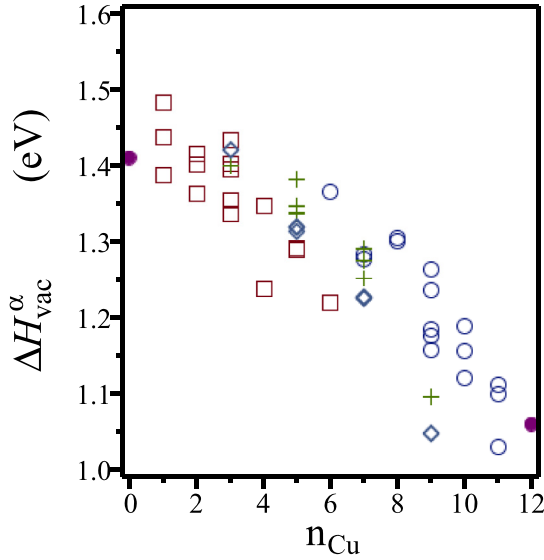


FIG. 2. (Color online) Vacancy formation enthalpy  $\Delta H_{\text{vac}}^\alpha$  as a function of the number of Cu atoms in the nearest neighbor shell ( $n_{\text{Cu}}$ ) as computed with Eq. (6) at various compositions; solid circles: in pure Cu and Ni; squares: in SQS-1 at  $x_{\text{Cu}} = 0.25$ ; crosses: in SQS-2 at  $x_{\text{Cu}} = 0.5$ ; diamonds: in SQS-3 at  $x_{\text{Cu}} = 0.5$ ; open circles: in SQS-1 at  $x_{\text{Cu}} = 0.75$ .

terms contribute to the formation enthalpy of a vacancy: (a) the energy to break the bonds between the vacated atom and its neighbor atoms and (b) the chemical potential of the vacated atom. The chemical potential represents the energy for putting the vacated atom back into the alloy, and this term makes the vacancy formation enthalpy composition dependent, see Eqs. (17). As the mixing enthalpy is concave with respect to composition in Cu-Ni, it follows that the chemical potential of Cu (Ni) decreases as the composition gets richer in Cu (Ni), see Fig. 7. In other words, putting back a Cu (Ni) atom in a Cu-rich alloy is less (more) costly than putting it back in a Ni-rich alloy. For this reason all the Cu-vacated vacancy formation enthalpies are rigidly shifted higher in  $\text{Cu}_{0.25}\text{Ni}_{0.75}$  in comparison to  $\text{Cu}_{0.75}\text{Ni}_{0.25}$ .

Of course the distinction between Cu and Ni vacancies is artificial: In the alloy one cannot know what atom has previously occupied the position of the vacancy site. Therefore, the  $\lambda$  Lagrange multiplier must be considered. Considering  $\text{Cu}_{0.50}\text{Ni}_{0.50}$  [Fig. 6(b)] it is clear that vacancies are most favorable at Ni occupied sites surrounded by many Cu atoms. The  $\lambda$  parameter makes sure that just as many Ni atoms get

TABLE IV. Effective cluster interactions (ECIs) in Cu-Ni system from cluster expansion.

| Cluster               | ECI (meV/cluster) |
|-----------------------|-------------------|
| $J_v$                 | 1505.5            |
| $J_{\text{Cu}}$       | 166.7             |
| $J_{v-\text{Cu}}$     | -53.5             |
| $J_{\text{Cu-Cu}}$    | -50.0             |
| $J_{v-\text{Cu-Cu}}$  | 4.08              |
| $J_{\text{Cu-Cu-Cu}}$ | 16.3              |

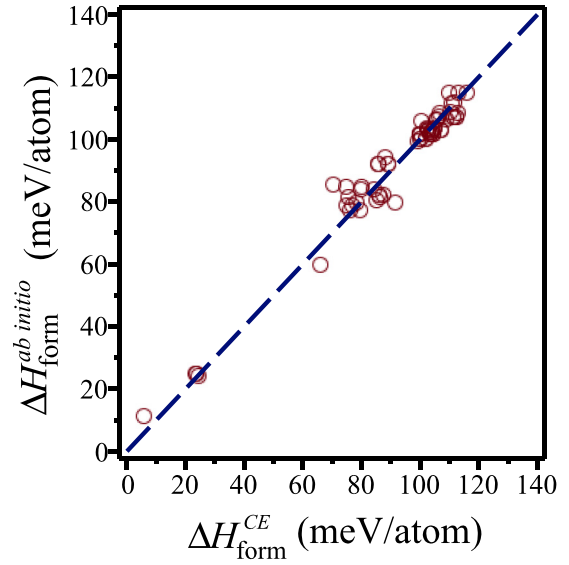


FIG. 3. (Color online) A comparison of formation energies calculated *ab initio* through Eq. (14) and as calculated with the cluster expansion.

vacated as Cu atoms (in an equiatomic alloy). Therefore, the  $\lambda$  parameter should make the Cu-vacated vacancies energetically a little less costly, and the Ni-vacated ones a little more costly. Equation (25) shows that this occurs when  $\lambda$  takes a negative value. At very high temperature, the Boltzmann factor for all vacancy types moves towards unity. Then, the combinatorial factor  $x_i^{(\alpha)}$  [Eq. (27)] plays a dominant role. For the random alloys this implies that  $\lambda$  moves towards zero, as is seen in Fig. 8. The  $\lambda$  parameter is a function of composition also. At

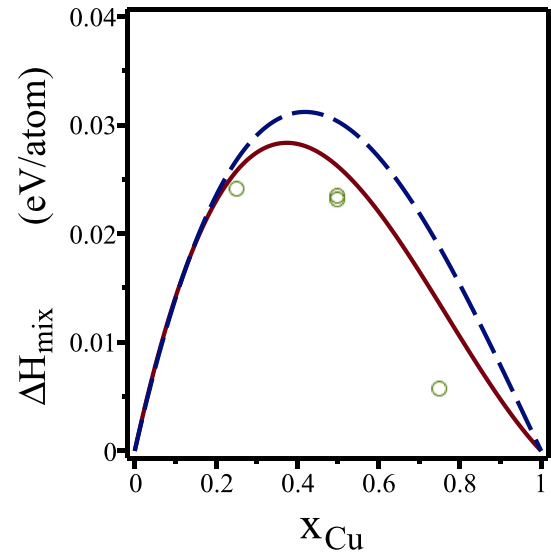


FIG. 4. (Color online) Mixing enthalpy of fcc Cu-Ni alloys as a function of the atomic fraction Cu; using the cluster expansion through Eq. (13) (solid line), using the SQS formation enthalpies from Eq. (14) (circles), and the mixing enthalpy at  $T = 298$  K as assessed on the basis of experimental data by an Mey [72] (dashed line).

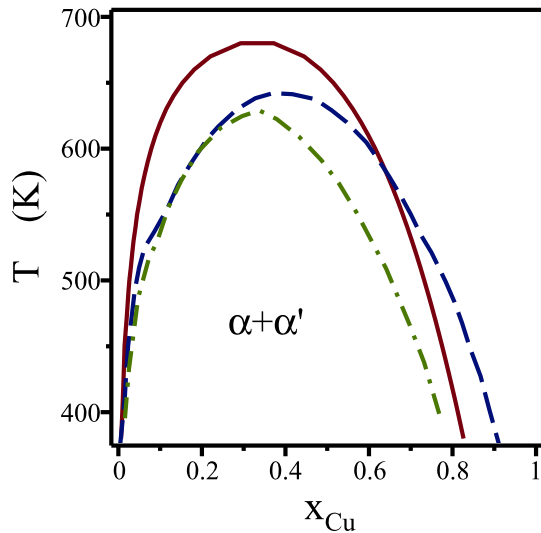


FIG. 5. (Color online) Low temperature part of Ni-Cu phase diagram as computed with the ECI in Table IV in the tetrahedron approximation of the CVM (solid line), as assessed by an Mey [72] (dashed line), and as assessed by Chakrabarti *et al.* [73] (dash-dotted line).

a given, not too high, temperature,  $\lambda$  is strongly negative at Ni-rich compositions while  $\lambda$  is weakly positive at Cu-rich compositions. Looking at Fig. 6(a), it is evident that the high Cu coordinated Ni sites are much more likely to be vacated in  $\text{Cu}_{0.25}\text{Ni}_{0.75}$  than in the equiatomic alloy, so that an even more negative  $\lambda$  value is required to balance Ni and Cu vacated sites. Figure 6(c), on the other hand, shows that for Cu-rich alloys the favorable high Cu coordinated Ni and Cu sites have about equal vacancy formation enthalpies. Therefore,  $\lambda$  must take very small values, and it needs to be slightly positive because the majority of vacancies must derive from Cu vacated sites.

Now that  $\lambda$  behavior has been rationalized, the total vacancy concentration  $x_{\text{vac}}(x_B, T)$  is examined. Figure 9 displays the Cu- and Ni-vacated vacancy concentrations  $x_{\text{vac}(i)}$  summed over all neighborhoods  $\alpha$ , and it shows the total vacancy concentration  $x_{\text{vac}} = x_{\text{vac}(\text{Ni})} + x_{\text{vac}(\text{Cu})}$ , as a function of the composition. Clearly, in the equiatomic alloy  $x_{\text{vac}(\text{Ni})} = x_{\text{vac}(\text{Cu})}$ , as imposed by the Lagrange multiplier  $\lambda$ . It is also obvious that at higher Cu content, the vacancy concentration is much larger because the vacancy formation energies decrease as the number of Cu nearest neighbors around a vacancy increases.

Fitting the total vacancy concentrations to an Arrhenius equation [Eq. (29)] yields the effective vacancy formation Gibbs energy  $\Delta G_{\text{vac}}^{\text{eff}}$ , see Fig. 10. It should be emphasized that only configurational excitations have been considered here so that for the pure elements ( $x_{\text{Cu}} = 0$ ,  $x_{\text{Cu}} = 1$ )  $\Delta G_{\text{vac}}^{\text{eff}}$  is found to be temperature independent.  $\Delta G_{\text{vac}}^{\text{eff}}$  is not well represented by a linear interpolation with respect to composition between the pure element values because it takes significantly lower values in concentrated alloys than the concentration weighted average. This is explained by the multitude of local neighborhoods that exist within an alloy, so that vacancies will be formed in the most favorable locations. Moreover, the deviation of  $\Delta G_{\text{vac}}^{\text{eff}}$  from the linear interpolated value  $\Delta G_{\text{vac}}^{\text{eff-xS}}$

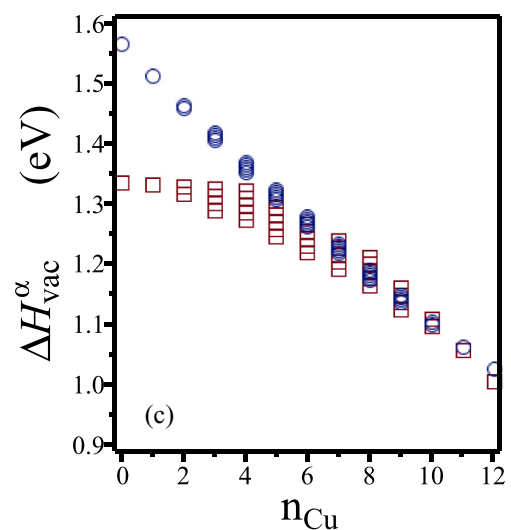
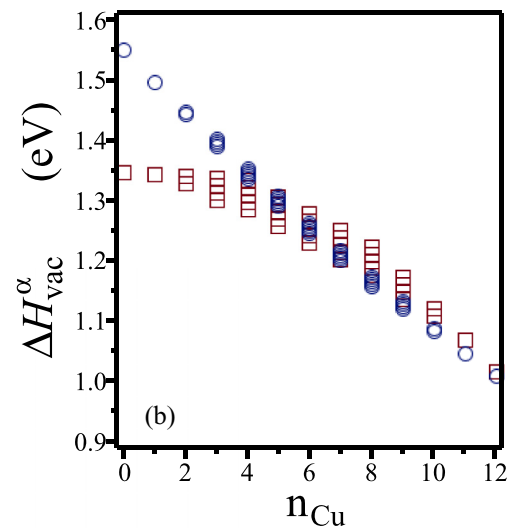
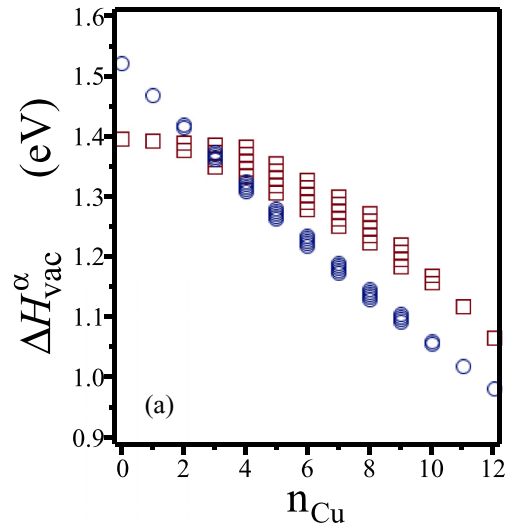


FIG. 6. (Color online) Vacancy formation enthalpy  $\Delta H_{\text{vac}(i)}^{(\alpha)}$  at  $T = 0$  K as a function of the number of Cu atoms in the nearest neighbor shell  $n_{\text{Cu}}$ , Ni-vacated (open circles), Cu-vacated (open squares): (a) in  $\text{Cu}_{0.25}\text{Ni}_{0.75}$ , (b) in  $\text{Cu}_{0.50}\text{Ni}_{0.50}$ , and (c) in  $\text{Cu}_{0.75}\text{Ni}_{0.25}$ .

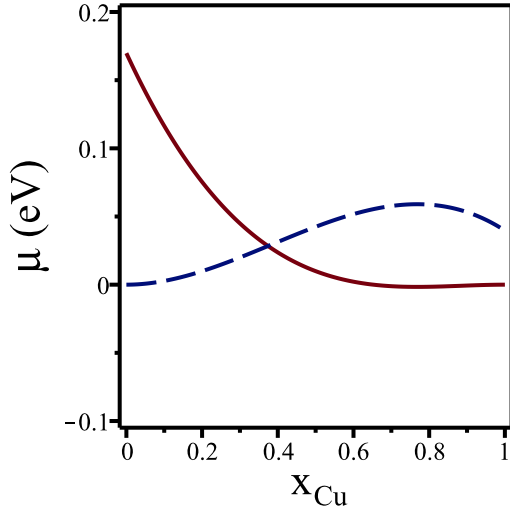


FIG. 7. (Color online) Chemical potential of Cu (solid line) and Ni (dashed line) as a function of composition at  $T = 0$  K.

gets smaller when temperature increases because there is then a weaker preference for low energy neighborhood vacancies. Nevertheless,  $\Delta G_{vac}^{eff-xS}$  remains negative for alloys with phase separation tendency. The high temperature limit of  $\Delta G_{vac}^{eff}$  is the statistical average of the vacancy formation enthalpy of all types of vacancies  $\sum_{\alpha,i} x_i^{(\alpha)} \Delta H_{vac(i)}^{(\alpha)}(x_{Cu})$ , which may be above the linear interpolation value for Cu-rich alloys.

In concentrated alloys,  $\Delta G_{vac}^{eff}$  increases with temperature which suggests a negative effective vacancy formation entropy  $\Delta S_{vac}^{eff}$ .  $\Delta S_{vac}^{eff}$  is computed with Eq. (30) using  $T_1 = 600$  K and  $T_2 = 1200$  K. The negative value of  $\Delta S_{vac}^{eff}$  too is a consequence of the multitude of local vacancy neighborhoods in concentrated alloys. At low temperature vacancies occur in the most favorable neighborhoods only, while at elevated temperature less favorable neighborhoods also provide vacancies. Of course this concerns the configurational aspect only. Nonconfigurational excitations, such as the vibrational

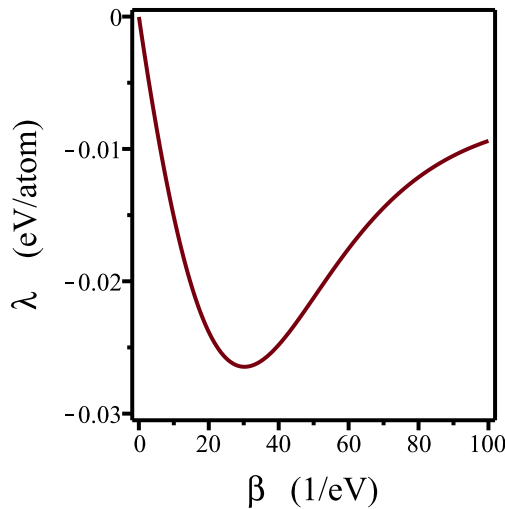


FIG. 8. (Color online) Lagrange multiplier  $\lambda$  in  $Cu_{0.50}Ni_{0.50}$  as given by Eq. (26) as a function of the inverse temperature  $\beta$ .

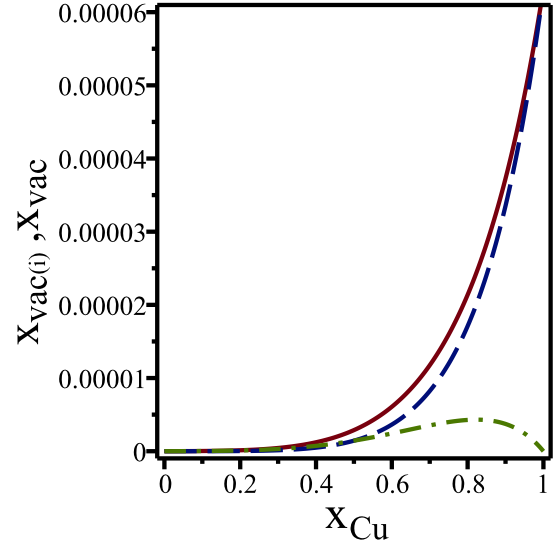


FIG. 9. (Color online) Vacancy concentration  $x_{vac(i)}$  (dashed line: Cu-vacated; dash-dotted line: Ni-vacated) and  $x_{vac}$  (solid line) at  $T = 1200$  K as given by Eq. (28) as a function of the Cu concentration  $x_{Cu}$ .

contribution to the entropy of vacancy formation, tend to give significantly positive effective vacancy formation entropy contributions, see, e.g., Table II in Ref. [11]. Nevertheless, the configurational contribution to  $\Delta S_{vac}^{eff}$  is quite large at about  $0.4k_B$  in  $Cu_{0.25}Ni_{0.75}$ , see Fig. 11. The magnitude of  $\Delta S_{vac}^{eff}$  is decided by the formation energy difference between vacancies at most and least favorable positions. For this reason,  $\Delta S_{vac}^{eff}$  increases when the vacancy formation energy in the pure end member elements differ strongly or when the SRO tendency gets stronger.

The effective vacancy formation enthalpy, as computed with Eq. (31), is displayed in Fig. 10. Like  $\Delta G_{vac}^{eff}$ , it shows

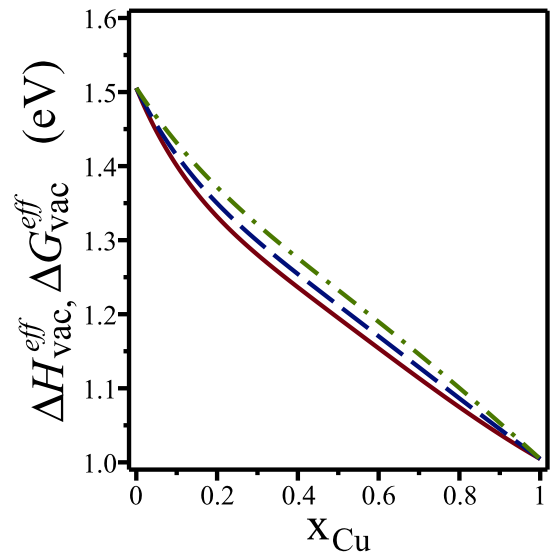


FIG. 10. (Color online) Effective vacancy formation enthalpy at  $T = 0$  K (solid line) and Gibbs energies at  $T = 600$  K (dashed line) and at  $T = 1200$  K (dash-dotted line) as a function of composition.

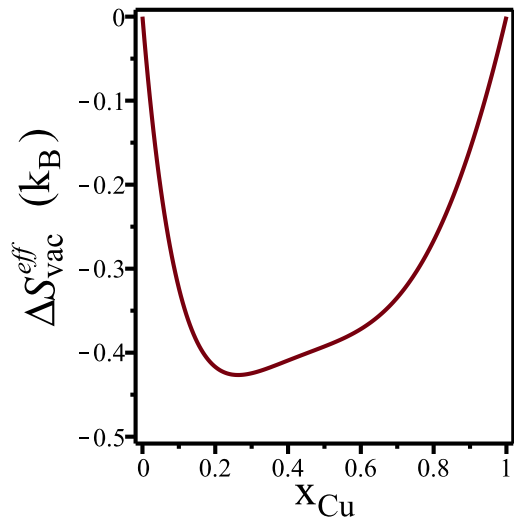


FIG. 11. (Color online) Effective vacancy formation entropy as a function of composition as computed with Eq. (30).

the strongest deviation from a linear composition dependence near  $x_{\text{Cu}} = 0.25$  because at the Ni-rich side the strongest shift of vacancy neighborhood occurs when the temperature is changed. At low temperature only high Cu coordinated vacancies can occur because they are energetically favored, but in a Cu-poor alloy such neighborhoods are rare. At high temperature also energetically much less favorable, but combinatorially much more prevalent, high Ni-coordinated vacancies occur. Thus in Ni-rich alloys the largest change in vacancy formation energies occurs as the temperature increases. This is illustrated in Fig. 12 where the average number of Cu nearest neighbors around a vacancy ( $n_{\text{Cu}}$ ) in  $\text{Cu}_{0.25}\text{Ni}_{0.75}$ , as computed with Eq. (32), is shown as a function of the inverse temperature  $\beta$ . In the vicinity of  $\beta = 0$ , the number of Cu neighbors converges to the random value of

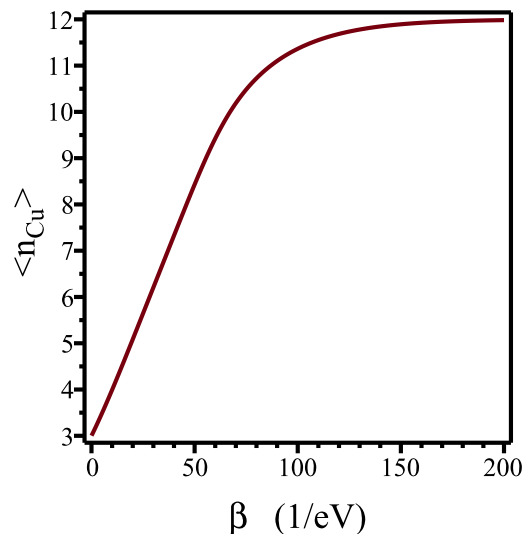


FIG. 12. (Color online) The average number of Cu neighbors around a vacancy ( $n_{\text{Cu}}$ ) in  $\text{Cu}_{0.25}\text{Ni}_{0.75}$  as a function of the inverse temperature  $\beta$ .

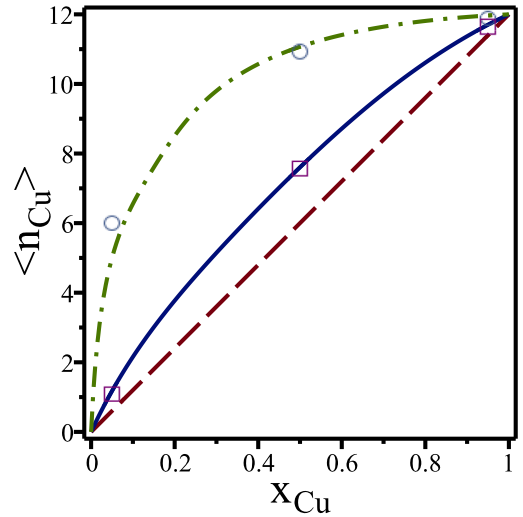


FIG. 13. (Color online) The average number of Cu neighbors around a vacancy ( $n_{\text{Cu}}$ ) at  $T = 200$  K (dash-dotted line), at  $T = 800$  K (solid line), and as extrapolated to infinite temperature (dashed line), as a function of the composition. The results predicted by Zhao *et al.* [24] are indicated as symbols:  $T = 200$  K data (circles);  $T = 800$  K data (squares).

$12 \times 0.25 = 3$ , but at large values of  $\beta$  vacancies occur only there where they are exclusively surrounded by 12 Cu atoms, in spite of Cu atoms being in the minority.

The strong preference of vacancies for Cu coordination occurs across the whole composition range, as is shown in Fig. 13. Our findings agree very well with an earlier embedded atom method (EAM) study [24], which included vibrational effects also. Apparently the vibrational effects play a minor role.

Instead of using the model introduced here, the CVM can be used to compute the vacancy concentration. The CVM in the tetrahedron approximation was used in conjunction with the CE listed in Table IV. The computed vacancy concentrations

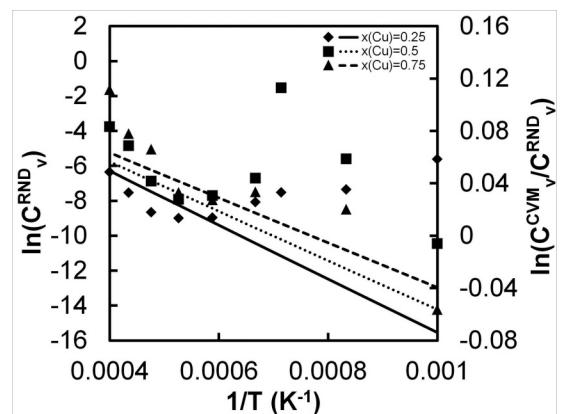


FIG. 14. Vacancy concentration  $C_v^{\text{md}}$  as computed with the current model as a function of inverse temperature  $\beta$  in  $\text{Cu}_{0.25}\text{Ni}_{0.75}$  (solid line),  $\text{Cu}_{0.5}\text{Ni}_{0.5}$  (dotted line), and  $\text{Cu}_{0.75}\text{Ni}_{0.25}$  (dashed line). Comparison between current model and CVM is indicated with symbols with reference to the axis on the right:  $\text{Cu}_{0.25}\text{Ni}_{0.75}$  (diamonds),  $\text{Cu}_{0.5}\text{Ni}_{0.5}$  (squares), and  $\text{Cu}_{0.75}\text{Ni}_{0.25}$  (triangles).



TABLE V. Effective cluster interactions (ECIs) in a hypothetical ordering A-B alloy.

| Cluster   | ECI (meV/cluster) |          |
|-----------|-------------------|----------|
|           | Case (a)          | Case (b) |
| $J_v$     | 2000              | 1200     |
| $J_B$     | -1200             | -1200    |
| $J_{v-B}$ | 16.7              | 83.3     |
| $J_{B-B}$ | 200               | 200      |

differ a few percent only from those computed with the current random model over a wide range of temperatures and compositions, see Fig. 14, in spite of the fact that the CVM includes the effect of short range order. The current model can be compared also with the quasichemical model as studied in much detail by Schapink [38]. The quasichemical approach too, like the CVM, yields vacancy concentrations that differ by a few percent from the values obtained with the current model. Other properties differ little between current and quasichemical, in the case of the vacancy formation free energy the difference is just 5 meV or less. In contrast to the earlier work [24,30,36,38], the current model can be implemented using a spreadsheet, no special software required.

**B. Alloy with ordering tendency**

It is of interest to examine whether the trends revealed for vacancy formation in phase separating alloys, such as Cu-Ni, also apply to alloys with ordering tendencies. Therefore, we examine an alloy with nearest neighbor pair interactions between A and B atoms such that the enthalpy of mixing at equiatomic composition is -300 meV/atom. These interactions, listed in Table V, are not *ab initio* and do not pertain to any real alloy system. They are selected to serve as illustration only. The interactions give the classical fcc phase diagram [74-77] for the solid state A-B alloy with a critical order-disorder

temperature of about 1100 K at equiatomic composition. Concerning the vacancy formation energies in pure A and B, we consider two cases: (a) the strong asymmetric case with vacancy formation energies in pure A (B) of 2 (1) eV and (b) the weak asymmetric case with vacancy formation energies in pure A (B) of 1.2 (1) eV.

The vacancy formation enthalpies  $\Delta H_{vac(i)}^{(\alpha)}$  at equiatomic composition as computed with Eqs. (17) are shown in Fig. 15. Due to the elimination of nearest neighbor equilateral triangle ECIs,  $\Delta H_{vac(i)}^{(\alpha)}$  of A-vacated and B-vacated vacancies for different  $\alpha$  have become linear functions of the number of B atoms in the nearest neighbor shell  $n_B$ , crossing at  $n_B = 6$ . Unlike a phase separating system like Cu-Ni, for a specific shell,  $\Delta H_{vac(i)}^{(\alpha)}$  of A-vacated vacancies is higher (lower) than that of B-vacated vacancies in B-rich (A-rich) shells because A-B bonds require more energy to be broken than the weighted average of A-A and B-B bonds. Furthermore, as expected, in case (b) the A and B vacated energies are much more similar than in case (a).

The effective Gibbs energy of vacancy formation,  $\Delta G_{vac}^{eff}$  [Eq. (29)] as function of the composition is curved upward, quite unlike the phase separating case, from the linear interpolation between the pure A and B end members. The deviation is rather similar in magnitude to the negative of the mixing enthalpy,  $-\Delta H_{mix}$ , both for case (a) and for case (b) (Fig. 16). As in the phase separating Cu-Ni alloy, the configurational contribution to the vacancy formation entropy [Eq. (30)] is negative. The reason for this is entirely the same as in the case of phase separation, at higher temperatures energetically less favorable configurations come into play.

The asymmetry in the end member vacancy formation energy does have a very pronounced effect on the short range order around a vacancy. Vacancy properties such as the configurational contribution to the entropy shift to a more negative value when the pure end member difference is larger (see Fig. 17).

Ordering systems, with interactions of the same magnitude as phase separating systems, develop vacancy-vacancy pairs

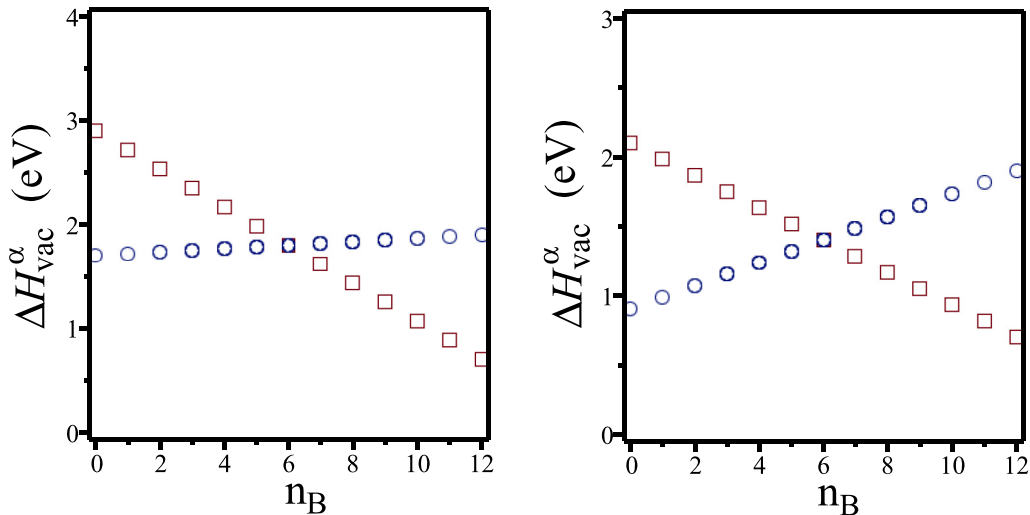


FIG. 15. (Color online) Vacancy formation enthalpy  $\Delta H_{vac(i)}^{(\alpha)}$  ( $x_B = 0.5$ ) at  $T = 0$  K according to Eqs. (17) as a function of the number of B atoms in the nearest neighbor shell  $n_B$ , A-vacated (open circles), B-vacated (open squares) vacancy. Panels correspond to cases (a) and (b) described in the text.

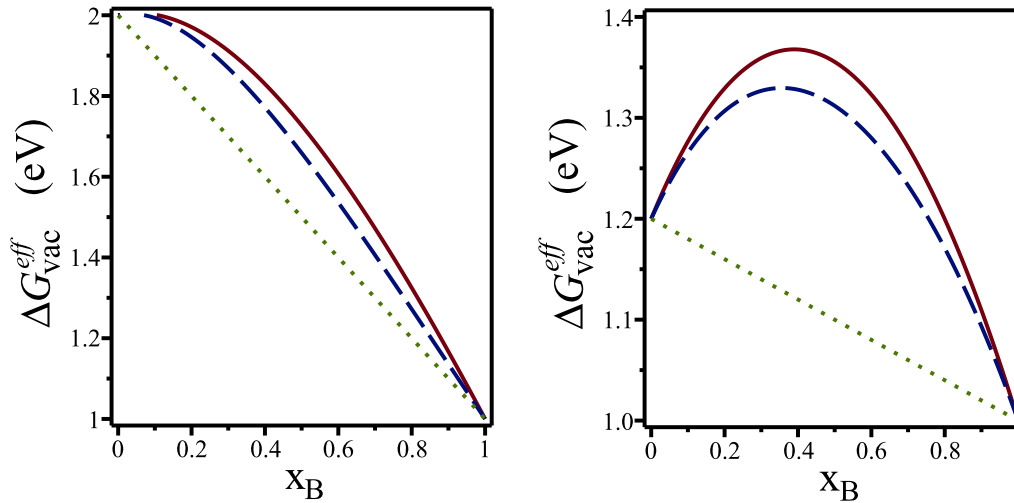


FIG. 16. (Color online) Effective vacancy formation Gibbs energy in an A-B ordering alloy as a function of the composition at  $T = 4000$  K (solid line) and  $T = 2000$  K (dashed line). Dotted line is the linear interpolation between the pure elements. Panels correspond to cases (a) and (b) described in the text.

already at a lower temperature. Therefore, the comparison between the current model and a more accurate methodology such as the cluster variation method or lattice Monte Carlo begins to break down at a lower temperature than was the case for phase separating systems. For alloys with ordering tendencies vacancy-vacancy pairs begin to play a role above about twice the highest order-disorder temperature.

## V. CONCLUSIONS

A formalism for the computation of vacancy formation energies in substitutional alloys has been presented. It is shown that composition and temperature play an important role in the thermodynamics of vacancies in alloys. The current approach, consisting of a cluster expansion coupled with a simple statistical thermodynamics model, has been shown

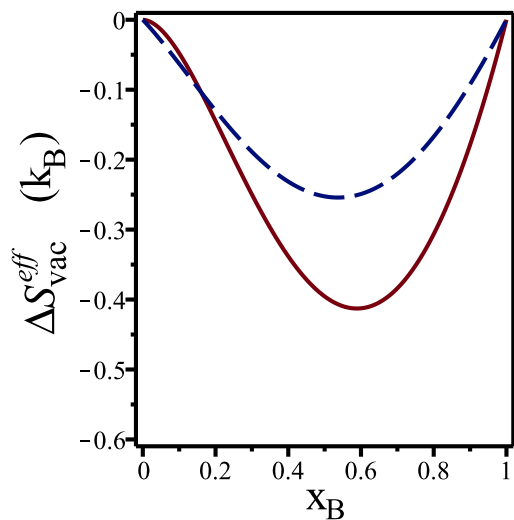


FIG. 17. (Color online) Effective vacancy formation entropy of an A-B ordering alloy as a function of composition: case (a) (solid line) and case (b) (dashed line).

to reproduce accurately the features of more sophisticated lattice gas models such as the quasichemical or cluster variation methods. The effective vacancy formation free energy deviates from the linear interpolation between that of the terminal pure phases in a manner opposite to the mixing enthalpy between those end members. Therefore, phase separating alloys have vacancy formation free energies that are less than the composition-weighted average of the end members, while the opposite holds in ordering type alloys. At low temperatures, the configurational contribution to the vacancy formation entropy is negative. This is caused by the fact that at low temperature vacancies will occur only in the energetically most favorable local neighborhoods in the alloy, while at higher temperatures also less energetically favorable neighborhoods come into play. In addition to ordering and phase separating tendencies, the asymmetry in the vacancy formation energy in the pure end members plays a significant role also. When the vacancy formation energies of the pure end members differ more strongly from one another, the excess vacancy properties in the alloy become more significant. Particularly, the configurational contribution to the entropy of vacancy formation becomes more negative, and the vacancy coordination departs stronger from the average, as the asymmetry in vacancy formation energies between the pure end members increases. In the current model pure vacancy clusters are not considered, so that at high temperature deviations from more accurate lattice gas models occur. These deviations are more significant for ordering type alloys than for phase separating alloys. It must be noted that in order to understand vacancy formation in substitutional alloys a few arbitrarily selected *ab initio* calculations on alloy supercells with vacancies generally will not suffice. A proper statistical thermodynamic analysis is required. As this work has shown, such a thermodynamic analysis need not be very complex fortunately.

Vacancies in the Cu-Ni system were shown to prefer Cu neighbors, regardless of the composition of the alloy. The vacancy formation free energy was shown to be strongly composition dependent, with lower values towards the Cu-rich

side. Since the vacancy formation energy in binary disordered alloys strongly depends on local environment, a cluster expansion was shown to be the optimal approach. Effective cluster interactions (ECIs) in terms of point, nearest neighbor pair, and nearest neighbor equilateral triangle clusters were extracted from a ternary cluster expansion by fitting the energies of 71 structures. The ECIs were used also to calculate the mixing enthalpy of the solid solution and the solid portion of the Cu-Ni phase diagram, which both agreed well with previous assessments. The CE approach coupled with a simple thermodynamic model made it possible to compute vacancy concentrations as a continuous function of temperature and composition. Fitting the vacancy concentration to an Arrhenius equation allowed us to extract the effective Gibbs energy of vacancy formation as a function of temperature and composition. The effective Gibbs energy of vacancy formation

was found to be a nonlinear function of composition with a deviation from linearity between the end members that was roughly equal to the negative value of the mixing enthalpy. The effective configurational entropy of vacancy formation was found to be composition dependent and negative with values ranging from about 0 to  $-0.5k_B$ .

## ACKNOWLEDGMENTS

One of the authors (M.S.) had the benefit of enlightening discussions with Professor Mike Finnis and Professor Jörg Neugebauer. The authors gratefully acknowledge financial support from China Scholarship Council (CSC, No. 2011637005).

- 
- [1] A. Janotti, M. Krčmar, C. L. Fu, and R. C. Reed, *Phys. Rev. Lett.* **92**, 085901 (2004).
- [2] C. Domain and C. S. Becquart, *Phys. Rev. B* **71**, 214109 (2005).
- [3] N. Sandberg and R. Holmestad, *Phys. Rev. B* **73**, 014108 (2006).
- [4] D. Simonovic and M. H. F. Sluiter, *Phys. Rev. B* **79**, 054304 (2009).
- [5] M. Mantina, Y. Wang, L. Chen, Z. Liu, and C. Wolverton, *Acta Mater.* **57**, 4102 (2009).
- [6] T. R. Mattsson, N. Sandberg, R. Armiento, and A. E. Mattsson, *Phys. Rev. B* **80**, 224104 (2009).
- [7] S. Huang, D. L. Worthington, M. Asta, V. Ozolins, G. Ghosh, and P. K. Liaw, *Acta Mater.* **58**, 1982 (2010).
- [8] S. Choudhury, L. Barnard, J. Tucker, T. Allen, B. Wirth, M. Asta, and D. Morgan, *J. Nucl. Mater.* **411**, 1 (2011).
- [9] K. M. Carling, G. Wahnström, T. R. Mattsson, N. Sandberg, and G. Grimvall, *Phys. Rev. B* **67**, 054101 (2003).
- [10] B. Grabowski, L. Ismer, T. Hickel, and J. Neugebauer, *Phys. Rev. B* **79**, 134106 (2009).
- [11] B. Grabowski, T. Hickel, and J. Neugebauer, *Phys. Status Solidi B* **248**, 1295 (2011).
- [12] C. L. Fu, Y.-Y. Ye, M. H. Yoo, and K. M. Ho, *Phys. Rev. B* **48**, 6712 (1993).
- [13] Y. Mishin and D. Farkas, *Philos. Mag. A* **75**, 169 (1997).
- [14] M. Hagen and M. W. Finnis, *Philos. Mag. A* **77**, 447 (1998).
- [15] B. Meyer and M. Fähnle, *Phys. Rev. B* **59**, 6072 (1999).
- [16] P. A. Korzhavyi, A. V. Ruban, A. Y. Lozovoi, Y. K. Vekilov, I. A. Abrikosov, and B. Johansson, *Phys. Rev. B* **61**, 6003 (2000).
- [17] J. Mayer, C. Elsässer, and M. Fähnle, *Phys. Status Solidi B* **191**, 283 (1995).
- [18] R. Krachler and H. Ipser, *Intermetallics* **7**, 141 (1999).
- [19] S. Foiles and M. Daw, *J. Mater. Res.* **2**, 5 (1987).
- [20] P. Ehrhart, P. Jung, H. Schultz, and H. Ullmaier, in *Atomic Defects in Metals*, edited by H. Ullmaier (Springer, Berlin, 1991), Vol. 25 of Landolt-Börnstein - Group III Condensed Matter.
- [21] Y. Kraftmakher, *Phys. Rep. Rev. Sec. Phys. Lett.* **299**, 80 (1998).
- [22] J. Dorn and J. Mitchell, *Acta Metal.* **14**, 70 (1966).
- [23] S. Tanigawa and M. Doyama, *Phys. Lett. A* **54**, 455 (1975).
- [24] B. L. Zhao, R. Najafabadi, and D. J. Srolovitz, *Philos. Mag. A* **70**, 519 (1994).
- [25] L. Zhao, R. Najafabadi, and D. Srolovitz, *Acta Mater.* **44**, 2737 (1996).
- [26] P. Venezuela, G. M. Dalpian, A. J. R. da Silva, and A. Fazzio, *Phys. Rev. B* **65**, 193306 (2002).
- [27] M. Muzyk, D. Nguyen-Manh, K. J. Kurzydłowski, N. L. Baluc, and S. L. Dudarev, *Phys. Rev. B* **84**, 104115 (2011).
- [28] E. del Rio, J. M. Sampedro, H. Dogo, M. J. Caturla, M. Caro, A. Caro, and J. M. Perlado, *J. Nucl. Mater.* **408**, 18 (2011).
- [29] J. B. Piochaud, T. P. C. Klaver, G. Adjanor, P. Olsson, C. Domain, and C. S. Becquart, *Phys. Rev. B* **89**, 024101 (2014).
- [30] F. Lechermann and M. Fähnle, *Phys. Rev. B* **63**, 012104 (2000).
- [31] A. Van der Ven and G. Ceder, *Phys. Rev. B* **71**, 054102 (2005).
- [32] A. Van der Ven and G. Ceder, *Phys. Rev. Lett.* **94**, 045901 (2005).
- [33] A. Van der Ven, H.-C. Yu, G. Ceder, and K. Thornton, *Prog. Mater. Sci.* **55**, 61 (2010).
- [34] G. L. W. Hart and A. Zunger, *Phys. Rev. Lett.* **87**, 275508 (2001).
- [35] W. M. Lomer, in *Vacancies and Other Point Defects in Metals and Alloys, Monograph and Report Series 23* (Institute of Metals, London, 1958), pp. 79–98.
- [36] L. Girifalco, *J. Phys. Chem. Solids* **25**, 323 (1964).
- [37] R. E. Howard and A. B. Lidiard, *Rep. Prog. Phys.* **27**, 161 (1964).
- [38] F. W. Schapink, *Philos. Mag.* **12**, 1055 (1965).
- [39] S. Masharov, *Sov. Phys. J.* **15**, 694 (1972).
- [40] S. M. Kim, *Phys. Rev. B* **30**, 4829 (1984).
- [41] A. R. Allnatt and A. B. Lidiard, *Atomic Transport in Solids* (Cambridge University Press, Cambridge, 1993).
- [42] O. Gorbato, P. Korzhavyi, A. Ruban, B. Johansson, and Y. Gornostyrev, *J. Nucl. Mater.* **419**, 248 (2011).
- [43] L. Delczeg, B. Johansson, and L. Vitos, *Phys. Rev. B* **85**, 174101 (2012).
- [44] A. Zunger, S.-H. Wei, L. G. Ferreira, and J. E. Bernard, *Phys. Rev. Lett.* **65**, 353 (1990).
- [45] S. B. Zhang and J. E. Northrup, *Phys. Rev. Lett.* **67**, 2339 (1991).
- [46] L. E. Ramos, J. Furthmüller, F. Bechstedt, L. M. R. Scolfaro, and J. R. Leite, *J. Phys. Condens. Matter* **14**, 2577 (2002).
- [47] P. C. Clapp, *Phys. Rev. B* **4**, 255 (1971).
- [48] J. Sanchez and J. Moran-Lopez, *Solid State Commun.* **79**, 151 (1991).
- [49] C. Wolverton and A. Zunger, *Phys. Rev. B* **57**, 2242 (1998).

- [50] F. Ducastelle and F. Gautier, *J. Phys. F* **6**, 2039 (1976).
- [51] M. H. F. Sluiter and Y. Kawazoe, *Phys. Rev. B* **51**, 4062 (1995).
- [52] M. H. F. Sluiter and Y. Kawazoe, *Phys. Rev. B* **68**, 085410 (2003).
- [53] G. Ceder, M. Asta, W. C. Carter, M. Kraitchman, D. de Fontaine, M. E. Mann, and M. H. F. Sluiter, *Phys. Rev. B* **41**, 8698 (1990).
- [54] P. A. Korzhavyi, L. V. Pourovskii, H. W. Hugosson, A. V. Ruban, and B. Johansson, *Phys. Rev. Lett.* **88**, 015505 (2001).
- [55] M. H. F. Sluiter and Y. Kawazoe, *Phys. Rev. B* **71**, 212201 (2005).
- [56] G. D. Garbulsky and G. Ceder, *Phys. Rev. B* **49**, 6327 (1994).
- [57] D. de Fontaine, in *Solid State Phys.*, Vol. 47, edited by H. Ehrenreich and D. Turnbull (Academic Press, New York, 1994), pp. 33–176.
- [58] J. Epperson, *J. Appl. Crystallogr.* **12**, 351 (1979).
- [59] J. W. D. Connolly and A. R. Williams, *Phys. Rev. B* **27**, 5169 (1983).
- [60] M. H. F. Sluiter, D. de Fontaine, X. Q. Guo, R. Podlucky, and A. J. Freeman, *Phys. Rev. B* **42**, 10460 (1990).
- [61] M. H. F. Sluiter and Y. Kawazoe, *Europhys. Lett.* **57**, 526 (2002).
- [62] J. P. Perdew, K. Burke, and M. Ernzerhof, *Phys. Rev. Lett.* **77**, 3865 (1996).
- [63] J. P. Perdew, K. Burke, and M. Ernzerhof, *Phys. Rev. Lett.* **78**, 1396 (1997).
- [64] G. Kresse and J. Furthmüller, *Comput. Mater. Sci.* **6**, 15 (1996).
- [65] G. Kresse and J. Furthmüller, *Phys. Rev. B* **54**, 11169 (1996).
- [66] G. Kresse and D. Joubert, *Phys. Rev. B* **59**, 1758 (1999).
- [67] M. H. F. Sluiter, Y. Watanabe, D. de Fontaine, and Y. Kawazoe, *Phys. Rev. B* **53**, 6137 (1996).
- [68] M. H. F. Sluiter, C. Colinet, and A. Pasturel, *Phys. Rev. B* **73**, 174204 (2006).
- [69] A. Glensk, B. Grabowski, T. Hickel, and J. Neugebauer, *Phys. Rev. X* **4**, 011018 (2014).
- [70] R. Armiento and A. E. Mattsson, *Phys. Rev. B* **72**, 085108 (2005).
- [71] A. Van de Walle, M. Asta, and G. Ceder, *CALPHAD* **26**, 539 (2002).
- [72] S. an Mey, *CALPHAD* **16**, 255 (1992).
- [73] D. J. Chakrabarti, D. E. Laughlin, S. W. Chen, and Y. A. Chang, in *Phase Diagrams of Binary Copper Alloys*, edited by P. R. Subramanian, D. J. Chakrabarti, and D. E. Laughlin (ASM International, Materials Park, OH, 1994), pp. 276–286.
- [74] C. van Baal, *Physica* **64**, 571 (1973).
- [75] R. Kikuchi, *J. Chem. Phys.* **60**, 1071 (1974).
- [76] J. M. Sanchez, D. de Fontaine, and W. Teitler, *Phys. Rev. B* **26**, 1465 (1982).
- [77] A. Finel and F. Ducastelle, *Europhys. Lett.* **1**, 135 (1986).
- [78] L. Delczeg, E. K. Delczeg-Czirjak, B. Johansson, and L. Vitos, *Phys. Rev. B* **80**, 205121 (2009).
- [79] R. Nazarov, T. Hickel, and J. Neugebauer, *Phys. Rev. B* **85**, 144118 (2012).
- [80] H.-E. Schaefer, *Phys. Status Solidi A* **102**, 47 (1987).
- [81] E. H. Megchiche, S. Pérusin, J.-C. Barthelat, and C. Mijoule, *Phys. Rev. B* **74**, 064111 (2006).